# A First Principles Approach to Investigation of the Role of Cations in Zeolite Growth and Stability

by

**Emily E. Freeman**

B.S. Chemical Engineering, University of South Carolina, 2018

Submitted to the Graduate Faculty of the

Swanson School of Engineering in partial fulfillment

of the requirements for the degree of

Master of Science in Chemical Engineering

University of Pittsburgh

2021

UNIVERSITY OF PITTSBURGH

SWANSON SCHOOL OF ENGINEERING

This thesis was presented

by

**Emily E. Freeman**

It was defended on

March 31, 2021

and approved by

Goetz Veser, PhD, Professor, Department of Chemical and Petroleum Engineering

Christopher Wilmer, PhD, Associate Professor, Department of Chemical and Petroleum Engineering

Thesis Advisor: Giannis Mpourmpakis, PhD, Associate Professor, Department of Chemical and Petroleum Engineering

**A First Principles Approach to Investigation of the Role of Cations in Zeolite Growth and Stability**

Emily E. Freeman, MS

University of Pittsburgh, 2021

Zeolites are porous aluminosilicate materials that find various applications in the chemical industry in separations, catalysis, ion exchange, etc. However, despite their widespread use, the reaction mechanisms occurring during zeolite growth are still unclear. Herein, we use Density Functional Theory calculations to gain insights into the thermodynamics of oligomerization, which constitute the initial steps of zeolite growth. By taking into consideration solvent and temperature effects, our results demonstrate that the growth of aluminosilicate systems is significantly more exothermic than their pure silicate counterparts. Under pH neutral conditions, water prefers to dissociate on the early-growth-stage aluminosilicate complexes rather than desorb, thus generating potential Brønsted acid sites on the oligomers. We take into consideration the role of cations during these first steps of growth as well as their role in the final zeolite product. These (alumino)silicate growth pathways are evaluated in the presence of $Na^+$ cation, as well as the $Ca^{2+}$ and $Zn^{2+}$ cations for the pure silicate pathway. The presence of cations increases the exothermicity of growth, with $Ca^{2+}$ exhibiting the most energetically favorable growth environment for the silicate systems. Importantly, we demonstrate through reaction extent analysis that the presence of cations modulates the speciation of the formed oligomers, with $Na^+$ favoring linear species in addition to the generally preferred cyclic ones. To further understand the energetic preference of cation localization in the final zeolite structure we perform a series of systematic cation substitution calculations as both framework and extraframework atoms. Overall, this work provides a

fundamental understanding of the thermodynamics of complex reaction paths that occur during early stages of zeolite growth and unravels thermodynamic preference of cation localization on final zeolite structure.

## Table of Contents

## List of Tables

## List of Figures

## Acknowledgements

I'd first like to thank Professor Giannis Mpourmpakis for his cherished guidance during this period of my life. I have grown academically, professionally, and personally under his mentorship and am extremely grateful for the time he has invested in my life. I'd like to thank my co-workers in the CANELa Lab, as their friendship and support has been so encouraging during my time at the University of Pittsburgh. Additionally, I'd like to thank my committee members, Professor Goetz Veser and Professor Chris Wilmer for their interest in my work and giving me the opportunity to learn from their expertise in their respective fields. I'd also like to thank my friends and family for always being a constant support system throughout my life and pushing me to become the best version of myself.

Finally, I'd like to thank those who funded the work that I've conducted during my Master's work. This work could not have been completed without support from the U.S. Department of Energy Nuclear Energy University Program (DOE-NEUP, Project Number 18-15496). The Pacific Northwest National Laboratory (PNNL), is a multiprogram national laboratory operated by Battelle for the U.S. DOE under Contract DEAC05-76RL01830. I would also like to acknowledge computational support from the Center for Research Computing (CRC) at the University of Pittsburgh.

## 1.0 Introduction

Zeolites are porous aluminosilicates that are both naturally occurring and synthetically produced. Zeolites are able be synthesized with detailed control of their physiochemical properties which makes them excellent materials for applications in fields such as separations[1], ion exchange [2], and catalysis [3]. The ability to control the structural and chemical functionalities of a given zeolite is extremely important for its end application. For example, ZSM-5 (MFI type) is one of the most commonly used industrial catalysts in the cracking of long hydrocarbon chains to produce light olefins due to its acidic properties and (hydro)thermal stability [4]. Additionally, zeolite growth has an important role in nuclear waste glass performance at disposal facilities. The adequacy of current methods of nuclear waste glass disposal is quickly becoming a topic of great interest with increased nuclear energy production[5]. In current practices, nuclear waste glass is stored in an underground repository where over time they begin to degrade. The formation of zeolites (specifically zeolites with GIS typology) has been shown to cause a delayed acceleration in the corrosion rate of certain glasses (Stage III), therefore it is essential that zeolite growth be well understood in order to be applied to control of waste glass corrosion [6-13]. Obtaining a detailed understanding of the mechanisms involved in early zeolite nucleation steps, and the effects of system composition on growth will enhance the ability to direct the phase of zeolite growth occurring in waste glass dissolution. The ability to control the rate and phase of zeolite growth as a means to manage nuclear waste glass corrosion has great potential to advance current practices in nuclear waste glass treatment.

Zeolite synthesis has significantly advanced over the years in terms of controlling their final structures; however, despite the progress that has been made in zeolite synthesis, the detailed

mechanisms for zeolite crystallization are far from being determined due to the complexity of their growth media. The largest gap in understanding how zeolites grow remains in the initial oligomerization steps of pre-nucleation (alumino)silicate species (oligomers, clusters, particles). The first steps of nucleation have been shown to have a large impact on the final topology of the zeolite[14]. These first steps determine which primary building units are formed, which determine which secondary building units are formed, which determine which zeolite topology the system can achieve. Therefore, gaining a deeper understanding of the mechanism(s) that drives these reactions is imperative to achieve better control during synthesis and eventually control the final zeolite structure. Such control would allow the development of novel zeolite structures, thus furthering the range of applications. Herein, we have sought to contribute to the work on these prevalent issues in the field of zeolites. This has resulted in portions of my thesis work being published in the AIChE Journal[15].

Many investigations, both experimental and computational, have attempted to clarify how initial oligomerization steps progress using several techniques such as nuclear magnetic resonance (NMR) [16], Density Functional Theory (DFT) calculations [17-22], and Monte Carlo simulations [21,23,24]. Experimental studies have offered insights into the effects of reactant composition and synthesis environment on the species formed during nucleation, which has direct impact on zeolite size, topology, and functionality [25]. However, it is difficult to experimentally observe the exact species (and their concentrations) formed during nucleation due to the extreme synthesis conditions (e.g. high ionic strength, pH, temperature, etc.), as well as the rate at which these reactions occur (< 1 s)[21] . On the other hand, deeper mechanistic understanding of early growth stages of materials can be achieved using DFT methods [26]. Specifically for zeolitic (alumino)silicate systems, studies have focused on probing mechanisms of the early oligomerization reactions, with extensive work being

done on the dimerization of silicates [20,27]; however, there is little consistency within these studies in terms of reactant species, simulated synthesis environment, solvation considerations, and reported energetics.

Several computational studies have probed the impact of pH on oligomerization in aluminosilicate systems, with most calculations being performed in the pH range of 8-11, where alkaline environments lend to the deprotonation of a given silanol group to facilitate further oligomerization [17,21]. This deprotonation step has resulted in a proposed anionic pathway of silicate oligomerization [27]. Systems that are highly alkaline (e.g. pH =11) have been shown to give preference to cyclic structure formation over their linear counterparts [28]. To better understand the role of solvent, the first oligomerization steps have been investigated using DFT calculations in various environments: the gas phase, implicitly solvated, explicitly solvated, and a combination of the latter two. White et al. [27] found that in order to obtain $pK_a$ values that were consistent with experimental data, it was necessary to use a combination of an implicit solvation model and explicit water molecules interacting with the structure of interest. This agrees with Catlow et al. who also showed that energies obtained using an implicit solvation model along with explicit solvent molecules were found to best agree with experimental values [29].

While the contributions of pH and solvation on the nucleation steps of zeolite growth have been addressed computationally [21], there remains a sizable gap in zeolite nucleation knowledge that has been untouched by computational studies. For instance, although zeolites are aluminosilicate materials, most of the computational studies focus only on oligomerization of pure silicate systems. Additionally, cations present in the synthesis environment can assume various roles during growth. Cationic species can perform as inorganic structural-directing agents, which serve to direct growth towards a desired structural conformation and can determine structural

characteristics in the final zeolite product [30]. Cations are also found in zeolites as counterions which stabilize charges in the zeolite framework that result from incorporation of aluminum. Though the effects of counterions in zeolite growth have been investigated previously [31-33], most computational studies focus on monovalent cations and rarely include divalent alkaline earth metals which are commonly found in natural zeolites.

Though cations are used extensively in zeolite synthesis, and are present in final zeolite products, the exact contributions of cations during growth as well as their position in the final zeolite product remain unclear. Cations present in a zeolite system are unique in that it is possible for their role to change dramatically from the stage of synthesis to the final stable product. The connection between initial composition and synthesis environment, and primary building units, secondary building units, and final zeolite product has been investigated previously and have confirmed a strong synthesis-structure relationship[34]. Knowing the location of the cations in the final zeolite product can lend to significant progress in the ability to direct and control the final zeolite product. Studies have been conducted previously to try to determine the final position of cations in several zeolite materials[35,36]. Not only can the location of these cations in a zeolite framework impact the energetics of the zeolite, they can also play a role in establishing the stability of a given state[37,38]. Several investigations have been conducted in attempt to elucidate the relationship between overall composition, primary and secondary building units, and environment, and the stability and interzeolite transformation of the product zeolite[39,40]. It is of great interest in the zeolite community, particularly the portion that involves nuclear waste glass treatment, that any potential method of directing interzeolite transformation by fully explored.

In the first portion of this work, we seek to understand aspects within early stages of zeolite growth that remain unclear. We use DFT calculations to gain a detailed understanding of the

energetic profiles of the initial steps of oligomerization in zeolite growth up to formation of the cyclic tetramer. To do so, we've investigated both pure silicate and aluminosilicate systems with resulting tetramer products containing Si/Al ratios of 1/1 or 3/1. Both linear and cyclic configurations are investigated for each oligomer (dimer, trimer, and tetramer), as larger cyclic oligomer species are considered to be important intermediates to the formation of zeolite building units [17]. In order to uncover the role of cations during early-growth stages, as well as probe their location on the small oligomer complexes, we have investigated the initial oligomerization steps in the presence of monovalent $Na^+$ (NaOH addition) and divalent $Ca^{2+}$ ($Ca(OH)_2$ addition) and $Zn^{2+}$ ($Zn(OH)_2$ addition) cations. In this work, we also address the preferred state of $H_2O$ molecules produced during oligomerization (condensation) reactions, which provides insight into the feasibility of forming Brønsted acid sites on aluminosilicate complexes during early growth stages. Additionally, we account for solvation environment and address temperature effects in the thermodynamic growth reaction profiles (free energy calculations). We evaluate not only the complexation thermodynamics of how zeolite precursor structures are formed prior to crystal growth, but we also provide insights into the role of cations and solvent on their structure and speciation.

In the second portion of this work, we investigate the preferential localization of cations in different positions of zeolite crystal framework cells. We use a Quantum Mechanics/Molecular Mechanics (QM/MM) method to explore cation substitution of zeolite cells. In these calculations we've substituted several cations $Al^{3+}$ ($Al(OH)_3(H_2O)$ addition), $Zn^{2+}$ ($Zn(OH)_2(H_2O)_2$ addition), and $Na^+$ ($Na(OH)(H_2O)_3$ addition) either as a framework cation on a tetrahedrally coordinated site within the framework, or as an extraframework cation substituting a Brønsted acid site. To be fully comprehensive we've performed these substitution calculations in both surface and bulk positions.

This provides information about the likelihood of a given cation to be present in a given position, as well as suggests the possibility of defects formation by controlling the synthesis conditions.

## 2.0 Computational Details

Density functional calculations were performed for silicate and aluminosilicate systems using the Gaussian 09 program package[41]. We used the M06-2X hybrid exchange-correlation functional [42] with the 6-311g(d,p) basis set. The M06-2X functional has been shown to perform well when tested against other popular functionals on calculating non-covalent bonding and thermochemistry of main group elements [43]. All calculations were performed using the conductor-like continuum model (CPCM) [44] as implemented in Gaussian to study the solvation effects, with water being the solvent. All species were fully optimized and frequency calculations were performed to verify that the structures are minima (absence of imaginary frequencies) and calculate Gibbs free energies (thermochemistry). DFT calculated free energies using the harmonic oscillator approach and implicit solvation conditions have been shown to produce results in good agreement with free energy values obtained using ab initio molecular dynamics [45]. To maintain charge consistency the systems were modeled to be in a pH neutral medium, which differs from experimental synthesis conditions where pH is commonly found to be 11-14. Under the typical pH range of zeolite synthesis, there would likely be anionic complexes formed during oligomerization. However, we selected pH neutral conditions in order to maintain a charge neutral growth system which does not require charge balancing counterions to provide charge stabilization, as well as to maintain reasonable computational cost. The inclusion of charge-balancing cations in the system would require the additional use of explicit $H_2O$ solvent molecules and would make the optimization of the systems challenging. Additionally, to accurately model anionic systems, the pKa value of each OH group in the system must be known, which is dependent on the overall complex configuration and can change for OH-groups in different environments[46]. A Quantum

Mechanics/Molecular Mechanics (QM/MM) method was used to explore cation substitution of zeolite cells. These substitution calculations were performed using ONIOM in Gaussian 09[41] using a two-layer approach. The density functional and basis set (M06-2X/6-311g(d,p)) used in small complex calculations were applied to the high layer atoms (consisting of Si, Al, Zn, Na, O, and H) in these systems. The semiempirical PM6 method[47] was assigned to the atoms (consisting of Si, O, and H) in the low layer. Two layering configurations were investigated, with the high layer applied to either select bulk or select surface atoms in a 354-atom zeolite crystal cell. In calculations exploring substitution in the bulk, only 17 atoms were included in the high layer region, with the remaining 337 atoms considered the low layer region. In the case of surface substitution calculations, 58 atoms were included in the high layer region, with the remaining 296 atoms being considered the low layer region. All zeolite substitution systems were conducted in the gas phase. All calculations, both oligomer and substitution were performed at 100°C, which is consistent with zeolite growth temperature conditions found in literature [48].

## 3.0 Results and Discussion

In order to develop a detailed mechanistic understanding of how zeolites grow, we focus on the initial oligomerization steps in (alumino)silicate systems. We have investigated the free energy pathways of these initial steps for both silicate and aluminosilicate systems, as shown in Figure 1. Appendix Figure 1 and Appendix Figure 2 display the Gibbs free energy and electronic energy reaction pathways, with each state labeled. The relevant structures of each state are presented in Appendix Figure 3. The Gibbs free energy includes enthalpic and entropic contributions to the total electronic energy. For each system, we have investigated oligomerization from the monomer, $Si(OH)_4$ and $Al(OH)_3$, up to formation of the cyclic tetramer complex.

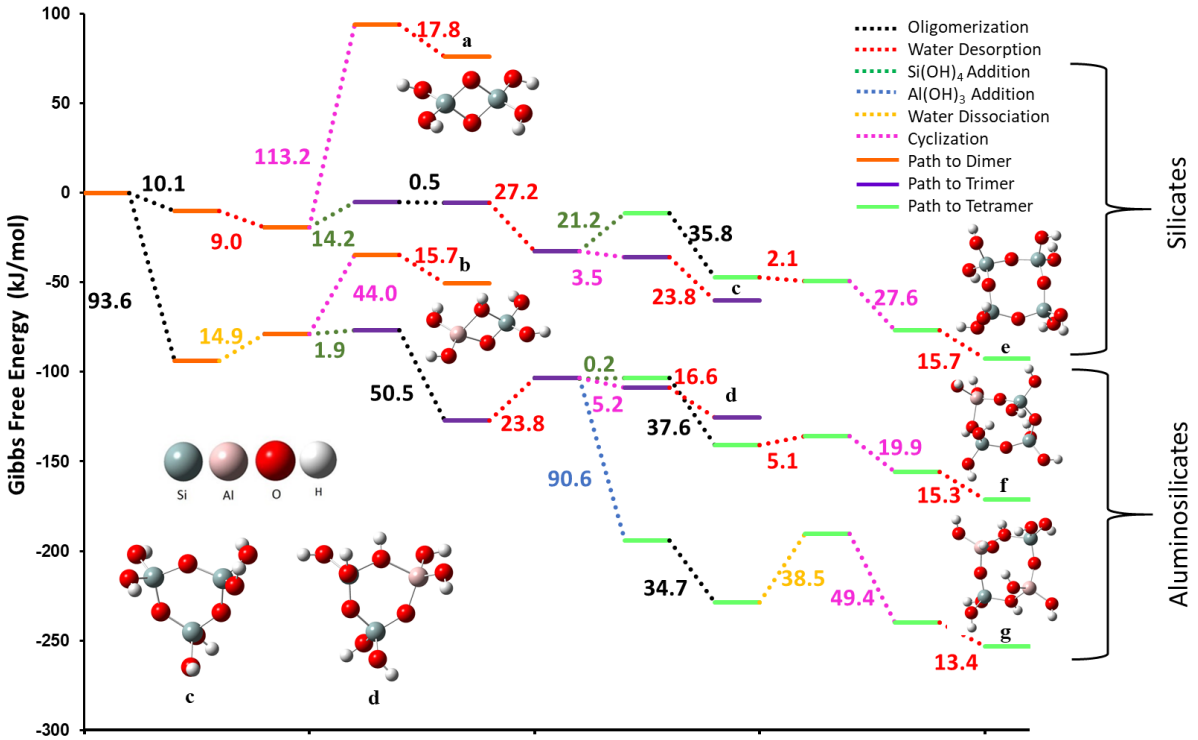


**Figure 1 Free energy reaction profile for oligomerization of silicate and aluminosilicate systems. The initial reactants for the silicate and aluminosilicate systems are Si(OH)4 + Si(OH)4 (top pathway) and Si(OH)4 + Al(OH)3 (bottom pathway), respectively. The num number listed by each step represents the absolute value of the change in Gibbs free energy between the two corresponding states (kJ/mol). Each number is color-coded to indicate the specific reaction step and is consistent with the coloring of the dashed lines. Colors of dashed lines in the figure indicate the following steps: black - oligomerization; red - water desorption; green - $Si(OH)_4$ addition; blue - $Al(OH)_3$ addition; yellow - water dissociation; and pink - cyclization. The solid lines are color-coded to highlight the paths forming oligomers of different size: orange – dimer species; purple – trimer species; and green – tetramer species. The profile shows the energetics for the formation of both the linear and cyclic structures through the tetramer. Terminal structures (states a-g) are shown for each pathway.**

### 3.1 Dimer Formation

The first oligomerization step is a condensation reaction between two monomers ($Si(OH)_4$ + $Si(OH)_4$, or $Si(OH)_4$ + $Al(OH)_3$) to form the dimers $Si_2O_7H_6(H_2O)$ or $SiAlO_6H_6(H_2O)$. Though the dimerization step in the silicate system is exothermic at -10.1 kJ/mol, the same step in the aluminosilicate system is significantly more exothermic at -93.6 kJ/mol. White et. al.[27] reports the same trend when comparing silicate and aluminosilicate dimerization at pH 11, with a silicate dimerization free energy of -1.8 kJ/mol, while the dimerization of its aluminosilicate counterpart ($Si(OH)_4$ + $Al(OH)_4^- \cdot Na^+$ as initial reactants) under the same conditions having a free energy of -21.2 kJ/mol. Furthermore, the silicate dimerization reaction step was reported to have a Gibbs free energy of -14.2 kJ/mol (at pH 7) by White et al. [27] and 0 kJ/mol by Mora-Fonz et al. [18], demonstrating that our numbers are within the reported range in literature. The energetic differences can be attributed to temperature and solvation effects. White et al. models solvation effects using the conductor-like screening model (COSMO) and includes explicit water molecules at a temperature of 298 K, whereas Mora-Fonz et al. reports energetics at 450 K using COSMO without considering explicit water molecules. In this work we evaluate these reactions at 373K using an implicit solvation model (CPCM) and include single explicit water molecules upon their formation during condensation reactions (oligomerization steps).

### 3.2 Trimer Formation

The next oligomerization step following formation of the dimer is the trimerization reaction. Here, a silicic acid monomer ($Si(OH)_4$) is added as reactant to with the linear dimer

($Si_2O_7H_6(H_2O)$ or $SiAlO_6H_6(H_2O)$ to produce a trimer product. Trimerization occurs after water desorption or water dissociation steps in the silicate and aluminosilicate systems, respectively. The trimer structures are shown in Appendix Figure 3 (labelled as structure 7 for the silicate system and 21 for the aluminosilicate system). The trimer $Al_2SiO_9H_8(H_2O)$ (with Si/Al ratio of 0.5) formed upon addition of aluminum hydroxide species ($Al(OH)_3$) was not considered in order to maintain a Si/Al molar ratio of 1 or greater, which is an attribute of many zeolite topologies, and remains in accordance with Löwenstein's rule which suggests the formation of Al-O-Al bonds is unfavorable in these systems [49]. The same trend found in the dimerization steps is also observed in the trimerization reactions. Trimerization of the aluminosilicate system was found to be more exothermic at -50.5 kJ/mol than its silicate counterpart at -0.5 kJ/mol. To our knowledge, there is little work reported in the literature on silicate trimerization [17,50], none of which has been conducted at 373 K. Trimerization in the silicate system at 450 K is reported by Mora-Fonz et al. [17] to be 6 kJ/mol (BLYP/DNP, COSMO), which again confirms our agreement with literature that silicate trimerization is relatively thermoneutral.

### 3.3 Tetramer Formation

The Si/Al molar ratios have been shown to have a direct impact on final zeolite structure and composition [51]. Therefore, two different Si/Al ratios for the aluminosilicate system were evaluated to examine the impact of aluminum and silicon composition on the energetics of oligomerization. In the aluminosilicate system, the growth path splits upon reactant addition to the trimer $Si_2AlO_{10}H_9$. The tetramer can be formed by adding either an $Si(OH)_4$, or an $Al(OH)_3$ monomer to the trimer complex, which can be seen in Appendix Figure 1 as the steps between

states 22 and 25 and 22 and 30, respectively. The addition of $Si(OH)_4$ produces a tetramer ($Si_3AlO_{13}H_{11}$) with an Si/Al ratio of 3, while the addition of $Al(OH)_3$ produces a tetramer ($Si_2Al_2O_{13}H_{12}$) with an Si/Al ratio of 1. The aluminosilicate tetramer complexes produced with the addition of $Si(OH)_4$ and $Al(OH)_3$ are shown in Appendix Figure 3 (as structures 27 and 32, respectively).

Tetramerization steps for all systems display similar energetics, with Gibbs free energies between -34 and -38 kJ/mol. At first glance, this suggests that the energetics of tetramerization are not strongly affected by the composition of the system; however, upon evaluation of the electronic energies we observe that this is not the case. In the silicate and aluminosilicate systems with Si/Al=3, the electronic energies were found to be -53.5 and -54.3 kJ/mol, respectively, whereas the electronic energy of the Si/Al=1 aluminosilicate system was found to be -35.8 kJ/mol. This indicates that entropic effects are more pronounced in systems where $Si(OH)_4$ is added to the trimer species ($\Delta S$ term is -0.041 kJ/mol·K for both pure silicate and Si/Al=3 tetramerization steps) rather than $Al(OH)_3$ ($\Delta S$ is -0.003 kJ/mol K for Si/Al=1 tetramerization). These effects are shown in Appendix Figure 2 as the steps between states 11-12, 25-26, and 30-31 for the silicate system, Si/Al=3 aluminosilicate system, and Si/Al=1 aluminosilicate system, respectively. This difference can be explained by the interaction between the water molecule produced during the formation of the aluminosilicate tetramer and the second aluminum atom (state 31 in Appendix Figure 1). Upon formation of the linear tetramer in the Si/Al=1 aluminosilicate system, the aluminum atom strongly interacts with the oxygen atom of the water molecule, which would explain why the entropic effects in this system are much smaller than in its counterparts. This can be seen in Appendix Figure 3 where reactant and product structures for the tetramerization steps are labeled as 11 and 12 for the silicate system, 25 and 26 for the Si/Al=3 aluminosilicate system, and 30 and 31 for

Si/Al=1 aluminosilicate system. Treatments of water molecules produced during condensation reactions will be discussed in greater detail in following sections.

### 3.4 Cyclization

Cyclization of (alumino)silicate complexes is critical to zeolite growth as many of the produced ring species are recognized as composite building units of zeolite framework structures [17]. The cyclization step occurs via a condensation reaction between the two ends of a linear chain, which produces a cyclic conformation of the oligomer complex and a water molecule. For both silicate and aluminosilicate systems, cyclization reactions were found to be favorable for the trimer and tetramer species, which is consistent with literature [17]. For both the silicate and aluminosilicate systems, we have investigated a configuration of the dimer species analogous to a cyclic configuration, where the two tetrahedral metal atoms share two oxygen atoms (shown respectively as states *a* and *b* in Figure 1, for silicate and aluminosilicate systems). The condensation steps necessary to form these dimer configurations are highly endothermic (113.2 and 44.0 kJ/mol in silicate and aluminosilicate systems, respectively) which suggests that they are unlikely to occur. Cyclization steps following dimerization were found to be exothermic. Gibbs free energies of trimer cyclization for the silicate (Figure 1, state *c*) and aluminosilicate (Figure 1, state *d*) systems are -3.5 and -5.2 kJ/mol, respectively. Tetramer cyclization was found to be the most exothermic of the cyclization reactions for all oligomer systems studied, which agrees with the observation that cyclic tetramer structures are common in several zeolite topologies. Cyclic tetramer structures are shown in Figure 1 as *e*, *f*, and *g* for the silicate, Si/Al=3 aluminosilicate, and Si/Al=1 aluminosilicate systems, respectively. The oligomerization paths explored in this work considers

oligomerization to occur in linear structures. Cyclization of linear oligomer structures produces terminal states in the growth pathway, therefore growth occurring on cyclic complexes is not investigated in this work.

### 3.5 $H_2O$ Desorption vs. $H_2O$ Dissociation in Aluminosilicates

To further understand how pre-nucleation species assemble and grow, we now focus on the step subsequent to an oligomerization step. Each oligomerization reaction produces an $H_2O$ molecule in addition to the (alumino)silicate complex. In order to maintain consistency in all calculations, the product $H_2O$ molecule was either desorbed (to the liquid phase) or dissociated on the complex, as shown in Figure 2. For the aluminosilicate system, we evaluated the energetics of the reaction path in the same step order (oligomerization step followed by $H_2O$ desorption step) as its silicate-only counterpart. We found the energetics of water removal steps in the aluminosilicate system to be significantly more endothermic than those of the silicate system. The $H_2O$ desorption step following the dimerization reaction in the aluminosilicate system (shown as step *a*-*b* in Figure 2) has a Gibbs free energy of +69.7 kJ/mol. That same water removal step in the silicate system has a value of -9.0 kJ/mol. Silicates are known to be hydrophobic, which is captured by the exothermic water desorption step. However, in the aluminosilicate system we observe an endothermic $H_2O$ desorption because upon $H_2O$ formation during oligomerization, the $H_2O$ molecule strongly associates with the aluminum atom on the aluminosilicate complex, which stabilizes the structure. This allows the aluminum atom to obtain its preferred tetrahedral coordination, which enhances the overall stability of the complex.

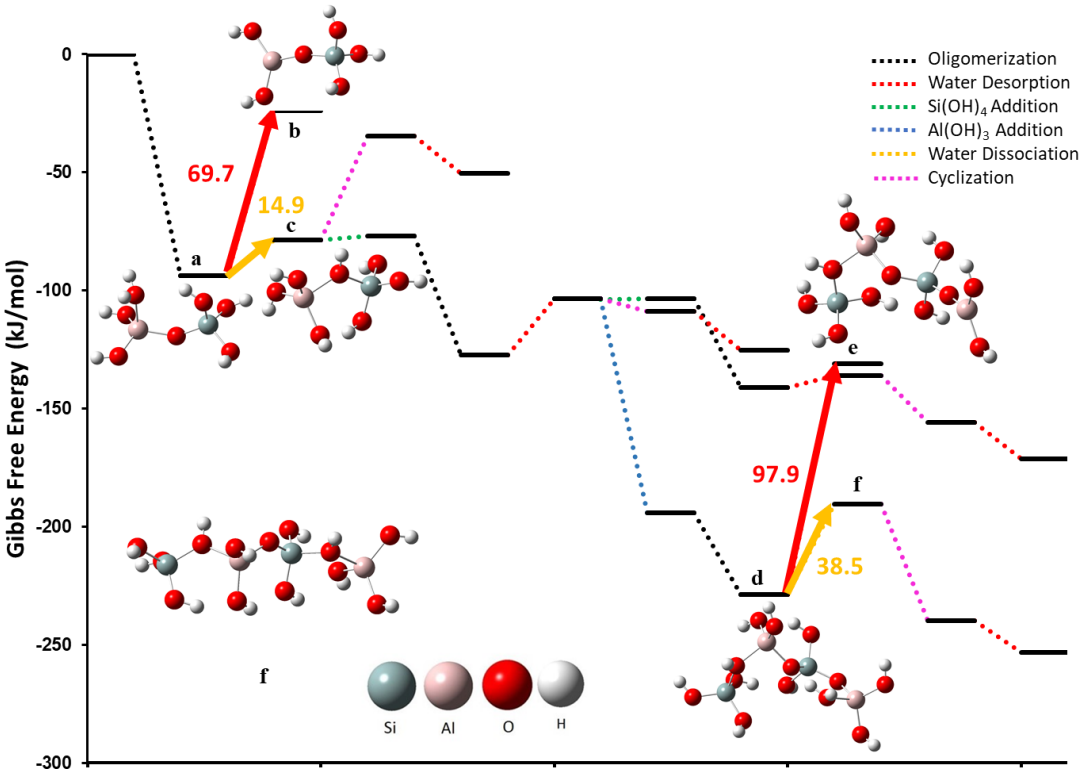


**Figure 2 Free energy reaction profile for oligomerization of the aluminosilicate system (note that this is a subset of information shown in Figure 1), demonstrating the energetics for water dissociation and water desorption after each Al(OH)3 addition. The water dissociation and desorption steps have been highlighted in red and yellow arrows, respectively. The number listed by each step represents the absolute value of the change in Gibbs free energy between the two corresponding states. Each number is color-coded to indicate the process that is occurring in that specific step and is consistent with the coloring of the dashed lines, details of which are given in Figure 1. Water prefers to dissociate on $SiAlO_6H_5$ and $Si_2Al_2O_{12}H_{10}$ rather than desorb, generating acidic hydrogens (Brønsted acid sites).**

To further address this thermodynamically unfavorable step in aluminosilicate systems, we explored the dissociation of water as an alternative to water desorption. Upon dissociation of the $H_2O$ molecule, a hydroxide group stays associated with the aluminum atom, while the remaining $H^+$ is bound to the bridging oxygen of the Si-O-Al bond, resulting in the formation of a Brønsted acid site. Figure 2 shows that the dissociation of $H_2O$ is energetically more favorable than $H_2O$

desorption for species where an $H_2O$ molecule interacts with an aluminum atom (highlighted in Figure 2 as red and yellow arrows, respectively). Appendix Figure 4 provides the free energy reaction diagram, with the structure corresponding to each labeled state provided in Appendix Figure 5. For the $H_2O$ desorption step following dimerization where the Gibbs free energy was found to be +69.7 kJ/mol (step a-b in Figure 2), the alternative option of dissociating the $H_2O$ molecule (*a* to *c*) exhibits a free energy of +14.9 kJ/mol, which is significantly less endothermic than water desorption. The same trend is observed following the oligomerization step forming the Si/Al=1 tetramer, in which $H_2O$ desorption (step *d* to *e*) has a free energy of +97.9 kJ/mol, and $H_2O$ dissociation (step *d* to *f*) is at +38.5 kJ/mol. This energetic preference of $H_2O$ dissociation over $H_2O$ desorption in the aluminosilicate system occurs due to the aluminum atom's preference to be tetrahedrally coordinated. By dissociating the water molecule, the aluminum atom remains tetrahedrally coordinated unlike in $H_2O$ desorption steps. Importantly, these observations indicate that Brønsted acid sites may be formed on intermediate species during these first steps of zeolite growth.

### 3.6 Cation Effect on Energetics of Silicate Growth

As an effort to elucidate the role of cationic species in the initial steps of zeolite growth, we have investigated how the thermodynamics of growth change in the presence of $Na^+$, $Ca^{2+}$, and $Zn^{2+}$. To this end, a proton on the $Si(OH)_4$ molecule was substituted with either $Na^+$, $Ca(OH)^+$, or $Zn(OH)^+$ (representing experimental NaOH, $Ca(OH)_2$, or $Zn(OH)_2$ addition, respectively) with the overall systems retaining their charge neutrality. We found that the presence of these cations ($Na^+$,

$Ca^{2+}$, and $Zn^{2+}$) shifts the reaction pathway to become more exothermic, as shown in Figure 3. Appendix Figures 6, 8, and 10 provide the free energy reaction diagrams, with the structures corresponding to each labeled state provided in Appendix Figures 7, 9, and 11 for the NaOH, $Ca(OH)_2$, and $Zn(OH)_2$ containing systems, respectively. Overall, we observe that the $Ca^{2+}$ oligomerization path is the most exothermic, followed in exothermicity by $Na^+$, then $Zn^{2+}$, and then the pure silicate. This is an interesting observation; taking into consideration that naturally formed zeolites typically contain $Ca^{2+}$ cations, here we demonstrate that the presence of $Ca^{2+}$ cations thermodynamically facilitate oligomerization. The dimerization reaction for silicate oligomerization in the absence of cations has a free energy of -10.1 kJ/mol, whereas this reaction in the presence of $Na^+$ becomes more exothermic with a free energy of -36.9 kJ/mol. Although the overall reaction path is most exothermic in the presence of $Ca^{2+}$, the respective dimerization step (second oligomerization step in $Ca^{2+}$ pathway) is less exothermic (compared to $Na^+$ and pure silicate paths) with a free energy value of -0.6 kJ/mol. This is particularly interesting considering the dimerization step in the presence of $Zn^{2+}$ (also divalent like $Ca^{2+}$) has a free energy value of 1.6 kJ/mol, which though similar to the dimerization step of the $Ca^{2+}$ system, the difference in the overall exothermicity of the paths is over 100 kJ/mol. The reduced exothermicity of the dimerization reaction in the presence of $Ca^{2+}$ and $Zn^{2+}$can be explained by the cation-oxygen interactions upon the addition of a $Si(OH)_4$ molecule. The formation of the Si-O-Si bond during dimerization decreases the number of silicon-bonded oxygens that $Ca^{2+}$ and $Zn^{2+}$ has available to interact with. These structures are provided in the Appendix as Appendix Figure 9 (labeled as state 5) for the $Ca(OH)_2$ system and as Appendix Figure 11 (labeled as state 5) for the $Zn(OH)_2$ system. The overall high exothermicity of the calcium-containing pathway can be partially explained by the exothermicity (-89.7 kJ/mol) of the substitution step, where $Si(OH)_4$ and $Ca(OH)_2$ react to form

the $Ca^{2+}$ substituted monomer $Si(OH)_3OCa(OH)$, depicted as state 3 in Appendix Figure 9. We see while observing the two divalent cation containing systems ($Ca^{2+}$ and $Zn^{2+}$) that the monomer oligomerization, subsequent $Si(OH)_4$ addition, trimer oligomerization, and tetramer oligomerization steps are all notably more exothermic for the $Ca^{2+}$ system than the $Zn^{2+}$ system. This suggests that the exothermicity of these systems are not dependent upon the valency of the cation. Neither the addition of $Na^+$, $Ca^{2+}$, or $Zn^{2+}$ produced a significant change in the energetics of dimer cyclization (edge-sharing tetrahedra configurations), which is endothermic for all systems. As shown in Appendix Figure 6, the edge-sharing dimer species $Si_2O_6H_3Na(H_2O)$, $Si_2O_7H_4Ca(H_2O)$, and $Si_2O_7H_4Zn(H_2O)$ have formation Gibbs free energies of 124.4, 171.6, and 123.3 kJ/mol, respectively. Structures for these complexes are shown in Appendix Figure 7 (state 7), Appendix Figure 9 (state 7), and Appendix Figure 11 (state 7) for the systems including $Na^+$, $Ca^{2+}$, and $Zn^{2+}$, respectively (results not shown in Figure 3 for clarity).

The introduction of divalent $Ca^{2+}$ or $Zn^{2+}$ into the silicate system was found to open an alternative oligomerization pathway. As a divalent atom, calcium (and zinc) can form two Ca-O (Zn-O) bonds and incorporate itself into the zeolite primary units formed during these initial steps, which could result in integration into the zeolite framework. This produces the formation of an O-Ca-O (O-Zn-O) bridge between two tetrahedral (Si, Al) atoms. Upon the addition of a second $Si(OH)_4$ to the Ca(OH) (Zn(OH)) substituted monomer ($Si(OH)_3OCaOH$; structure 3 in Appendix Figure 9, or $Si(OH)_3OZnOH$; structure 3 in Appendix Figure 11) the pathway splits to form either a Si-O-Si bond (shown in Appendix Figure 8 as the step between states *4* and *5* for the $Ca^{2+}$ system; Appendix Figure 10 as the step between states *4* and *5* for the $Zn^{2+}$ system ) or an O-Ca-O (O-Zn-O) bond (shown in Appendix Figure 8 as the step between states *4* and *9* for the $Ca^{2+}$ system; Appendix Figure 10 as step between states 4 and 9 for the $Zn^{2+}$ system). These complexes

are shown in Appendix Figure 9 as structures 5 and 9 for the species with Si-O-Si and O-Ca-O, respectively (Appendix Figure 11 as structures 5 and 9 for Si-O-Si and O-Zn-O, for the Zn system). We investigated all reaction steps in the silicate systems containing $Ca^{2+}$ and $Zn^{2+}$ (with the exception of the cyclic dimer) using structures that contain an O-Ca-O or O-Zn-O bond rather than structures that include an O-Ca-OH or O-Zn-OH bond. It is also worth noting that in addition to zeolites, calcium silicates also play an important role in the composition of Portland cement, and thus have significant environmental impact[52]. There has been much work done in the field of cement science that seeks to optimize cement composition, improve cement hydration rates, and in turn lower the carbon footprint of global cement use[53-55].

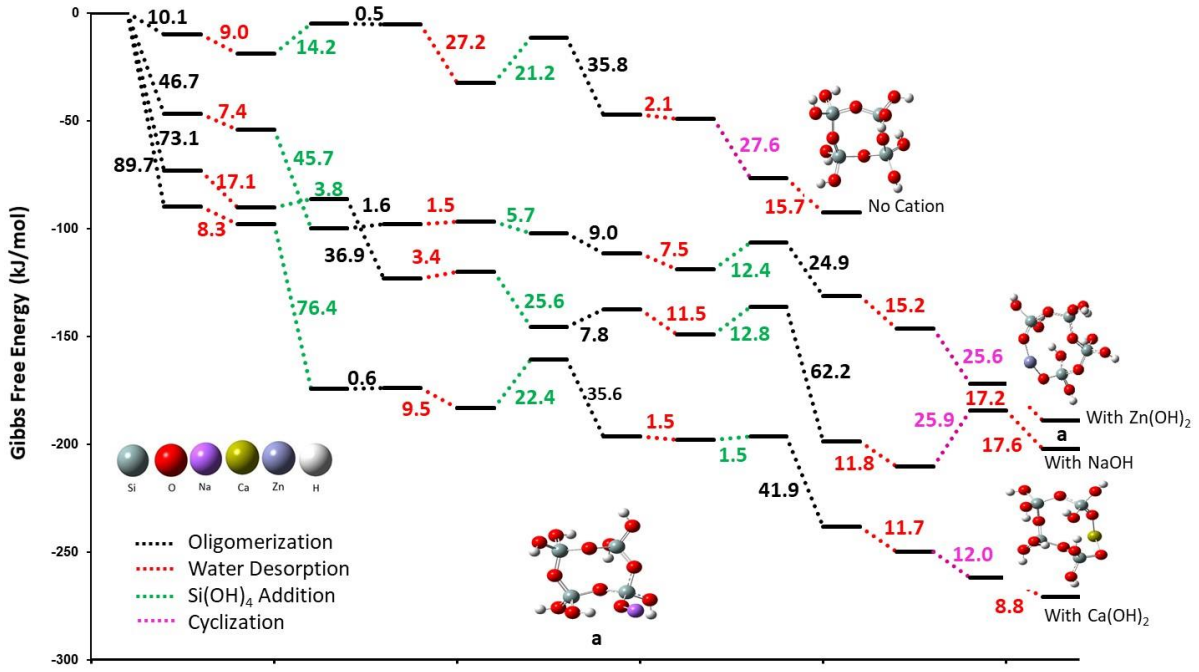


**Figure 3 Free energy reaction profiles for oligomerization of silicates in the absence and presence of Na+, Ca2+, and Zn2+ cations (NaOH, Ca(OH)2, and Zn(OH)2 addition). The initial reactants for the systems are Si(OH)4 + Si(OH)4, Si(OH)4 + NaOH, Si(OH)4 + $Ca(OH)_2$, and $Si(OH)_4$ + $Zn(OH)_2$, respectively. The number listed by each step represents the absolute value of the change in Gibbs free energy between the two corresponding states. Each number is color-coded to indicate the process that is occurring in that specific step and is consistent with the coloring of the dashed lines, details of which are given in Figure 1. The solid lines**

**are color-coded to highlight the paths forming oligomers of different size as in Figure 1. The profile shows the energetics for the formation of both the linear and cyclic structures for each species through the tetramer. Terminal structures are shown for each pathway.**

### 3.7 Cation Effect on Energetics of Aluminosilicate Growth

Following the approach used to explore the effects of cations on the reaction pathway of silicate oligomerization, the impact of $Na^+$ and $Zn^{2+}$ was also investigated in the aluminosilicate systems (Figure 4). Appendix Figures 12 and 14 provide the free energy reaction diagram with each state labeled for the $Na^+$ and $Zn^{2+}$ systems, respectively. Here we substitute the cation onto the $Al(OH)_3$ molecule rather than $Si(OH)_4$, forming the $Al(OH)_2ONa$ and $Al(OH)_2OZn(OH)$ monomers (Appendix Figure 13, state 3 and Appendix Figure 15, state 3, respectively). In the case of the zinc containing system, the substitution of $Zn^{2+}$ on $Al(OH)_3$ is preferred (78.2 kJ/mol, Figure 4) over substitution on $Si(OH)_3$ (46.7 kJ/mol, Figure 3). Though the substitution of $Na^+$ on $Si(OH)_4$ is thermodynamically preferred (-73.1 kJ/mol, Figure 3) over substitution on $Al(OH)_3$ (-30.8 kJ/mol, Figure 4), the aluminosilicate system containing sodium is evaluated starting from the substituted $Al(OH)_3$ complex ($Al(OH)_2ONa$) for consistency with the $Zn^{2+}$ system (starting with $Al(OH)_2OZn(OH)$). We chose to evaluate this pathway in order to understand the effects of aluminosilicate growth when the cation is substituted on $Al(OH)_3$, which is compared with the respective growth energetics when the cation is substituted on $Si(OH)_4$ groups (Figure 3). Despite there being some differences in the energetics of the individual steps along the growth path, the overall thermodynamics converge upon formation of the dimer when in both systems we consider the $Na^+$ atom to be positioned on the bridging oxygen, which results in the same dimer product

regardless of which tetrahedral atom (Si, Al) the $Na^+$ is first associated with. We observe that $Na^+$ behaves as an aggregation center for the small aluminosilicates, which promotes the growth of larger oligomer complexes.

As discussed above, a condensation reaction involving $Al(OH)_3$ is followed by a $H_2O$ dissociation step, forming a Brønsted acid site on the bridging oxygen. In aluminosilicate systems containing $Na^+$ counterions, we consider the $Na^+$ atom to take the place of the $H^+$ on the acid site (similar to ion exchange), whereas in the case of $Zn^{2+}$ the cation takes a bridging position in the framework as it does in the silicate systems discussed previously. In this $Na^+$ case, the $Al(OH)_2ONa$ molecule reacts with a $Si(OH)_4$ monomer, forming an Al-O-Si bond with $Na^+$ positioned on the bridging oxygen atom (similar to positions assumed by extra-framework cations in zeolites). In the same step a hydroxide group coordinates with the aluminum atom producing the dimer complex $AlSiNaO_7H_6$ (structure 5 in Appendix Figure 13), where the aluminum atom is tetrahedrally coordinated and $Na^+$ is stabilized on a bridging oxygen of the dimer, resulting in a highly exothermic (-292.1 kJ/mol) oligomerization step. As we have only added one cation (NaOH or $Zn(OH)_2$) molecule to our systems, the $Na^+$ atom is associated with the position that was the Brønsted acid site in the pure aluminosilicate system. In the case that we form the tetramer with a Si/Al ratio of 1 (i.e., presence of 2 Al atoms), the additional negative charge of the oligomer is counterbalanced by $H^+$ occupying the oxygen bridging the silicon and aluminum atoms. This produces an aluminosilicate tetramer (shown in Appendix Figure 13 as state 20) that contains both a typical Brønsted acid site and a $Na^+$ cation that is associated with a bridging oxygen.

Consistent with what was observed in the silicate system, the growth pathways of the aluminosilicate system are found to become more exothermic in the presence of a cation. The NaOH containing system was found to be the most overall exothermic when compared to its

$Zn(OH)_2$ containing and pure (alumino)silicate counterparts. In all three systems, the pathway to tetramer formation with a Si/Al ratio of 1 is more energetically favorable than tetramer formation with a Si/Al ratio of 3. One important observation made for the (alumino)silicate systems is that the $Zn^{2+}$ containing systems seem to limit growth to the trimer, whereas $Na^+$ seems to promote growth past the trimer. In the $Zn^{2+}$ containing system, upon formation of the trimer the addition of $Si(OH)_4$ (to form tetramer product with Si/Al of 3) is an endothermic step with a Gibbs free energy 34.6 kJ./mol and is closely followed by a water desorption step and tetramer cyclization step, both endothermic with Gibbs free energy values of 45.1 and 57.9 kJ/mol, respectively. When evaluating the path to formation of a tetramer species with Si/Al ratio of 1 for the $Zn^{2+}$ containing system, we see that there are also endothermic steps on this path (tetramer oligomerization and water dissociation with Gibbs free energies of 28.4 and 24.0 kJ/mol, respectively) that may limit the formation of the tetramer product. The $Na^+$ containing system has significantly lower thermodynamic limitations, thus promoting formation of the tetramer product. Interestingly, we see that in the case of the $Zn^{2+}$ system the first the $H_2O$ dissociation step (directly following $Zn^{2+}$ substitution on the $Al(OH)_3$ monomer) becomes significantly exothermic (-114.9 kJ/mol), whereas almost all $H_2O$ dissociation steps in all other systems are endothermic. This could be due to enhanced interactions between the $Zn^{2+}$ cation and surrounding oxygen atoms and additional hydrogen bonding interactions (Appendix Figure 14, state 9) upon water dissociation.

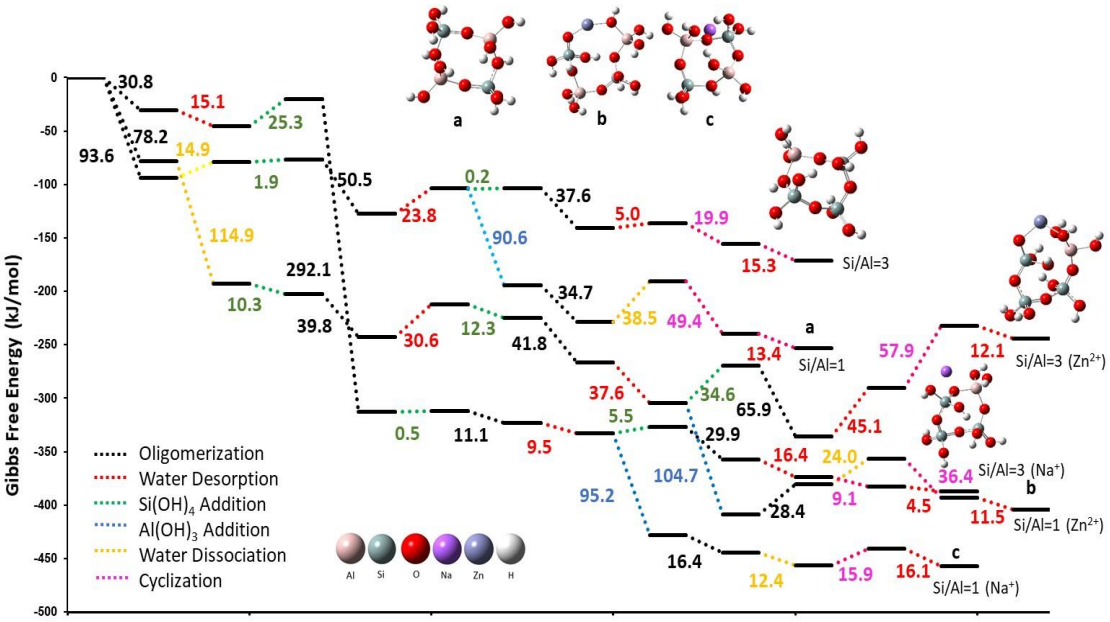


**Figure 4 Free energy reaction profile for oligomerization of aluminosilicate system in the absence and presence of NaOH and $Zn(OH)_2$. The initial reactants for the systems are $Si(OH)_4$ + $Al(OH)_3$ (-93.6 kJ/mol), $Al(OH)_3$ + Na(OH) (-30.8 kJ/mol), and $Al(OH)_3$ + $Zn(OH)_2$ (-78.2 kJ/mol), respectively. The number listed by each step represents the absolute value of the change in Gibbs free energy between the two corresponding states. Each number is color-coded to indicate the process that is occurring in that specific step and is consistent with the coloring of the dashed lines, details of which are given in Figure 1. The solid lines are color-coded to highlight the paths forming oligomers of different size as in Figure 1. The profile shows the energetics for the formation of both the linear and cyclic structures for each species through the tetramer. Terminal structures are shown for each pathway.**

## 3.8 Reaction Extent Analysis

Quantification of species in solution has been a well-investigated topic in the materials growth field for many years. Many approaches, both experimental and computational, such as NMR[56,57], Kinetic Monte Carlo[58], Mass Spectrometry[59,60], etc. have been employed to quantify the

species present in a growth environment. Pelster et. al. investigated the species present during synthesis of various pure-silicate zeolites using Mass Spectrometry[60]. The most prevalent species found in the synthesis media was a 32-unit oligomer, however, they also detected the presence of smaller 6- and 8-unit species at lower concentrations. Kirschhock et. al. performed a study using NMR and infrared spectroscopy to identify the polycondensation products formed during growth of the MFI zeolite, where the most predominant species was a 33 Si atom complex[57]. Several smaller species were also observed at various times throughout the synthesis such as the three-ring, bicyclic pentamer, and double five-ring complexes (five-ring containing species are common in the MFI topology). Experimentally determining the species present at these very initial stages of growth remains challenging due to the small size of the pre-nucleation species, fast time-scales of nucleation, and complex growth environment. It is also worth noting that both aforementioned studies have different synthesis conditions (temperature, time-scale, reactant materials, etc.), which can have significant impact on the species found during growth.

Here, in an effort to determine if early growth will be limited by the endothermic steps on the reaction pathways and find the relative concentrations of each species along the reaction pathway, a reaction extent analysis was performed. Each pathway was evaluated individually in order to determine which species were most prevalent for each system under thermodynamic equilibrium at 373K. For the three silicate systems shown in Figure 5A, each calculation was performed with an initial Si concentration of 4 mol, and 1 mol for the cation reactant species, NaOH or $Ca(OH)_2$. The four aluminosilicate pathways, displayed in Figure 5B, had initial concentrations (Si:Al:Na) of 3:1:0, 2:2:0, 3:1:1, and 2:2:1 for aluminosilicate Si/Al=3, aluminosilicate Si/Al=1, aluminosilicate with $Na^+$ and Si/Al=3, and aluminosilicate with $Na^+$ and Si/Al=1, respectively. Additional details on the reaction extent calculations can be found in the

Appendix. The percentages reported in Figure 5 correspond to the Si-content converted to products with respect to the initial Si of the system.

The silicate system in the absence of cations (red pathway in Figure 5A) was found to proceed until 97% of initial Si was converted to the cyclic tetramer complex (Figure 5A, state c). Upon the addition of NaOH (purple pathway in Figure 5A), 91% of initial Si was converted to the linear tetramer complex (Figure 5A, state e), with only 1% of initial Si progressing to the cyclic tetramer (Figure 5A, state f). This indicates that the endothermic tetramer cyclization step (25.9 kJ/mol) limits growth past the linear tetramer in the presence of NaOH. The silicate with $Ca(OH)_2$ produced two complexes, 22% for the cyclic tetramer—$H_2O$ (hydrated complex) and 78% of the cyclic (dehydrated) tetramer (hydrated and dehydrated states shown in Figure 5A as states g and h, respectively). Structures corresponding to states labeled a-c in Figure 5A can be found in Appendix Figure 3 labeled as structures 1A, 14 and 15. Similarly, the structures corresponding to states labeled d-f in Figure 5A can be found in Appendix Figure 7 as structures 15-16, and 18, and states labeled g-h in Appendix Figure 9 as structures 19-20.

As shown in Figure 5B, the aluminosilicate system and aluminosilicate system with $Na^+$, for pathways with Si/Al=3 (red and purple paths, respectively), the cyclic tetramer species (Figure 5B, states b and g, respectively) were most prevalent with 98% total Si content in each case. For the Si/Al=1 pathway involving pure aluminosilicate, the cyclic tetramer (Figure 5B, state e) and linear tetramer—$H_2O$ (Figure 5B, state c) complexes were found at concentrations of 42% Si and 57% Si, respectively. Similarly, the Si/Al=1 pathway for the aluminosilicate system with $Na^+$ is also split with the cyclic tetramer (Figure 5B, state j) and linear tetramer (Figure 5B, state i) complexes, with Si concentrations of 50% and 49%, respectively.

The key difference between the two Si/Al=1 pathways is that in the pure aluminosilicate system, the $H_2O$ molecule produced during tetramerization is still associated with the linear tetramer, whereas in the system of aluminosilicate with $Na^+$, the prevalent species is the linear tetramer with water dissociated. This can be attributed to the respective $H_2O$ dissociation steps being exothermic (-12.4 kJ/mol) in the $Na^+$ containing system and endothermic (38.5 kJ/mol) in the pure aluminosilicate system. In the case of the $Na^+$ containing aluminosilicate system with Si/Al=1, the tetramer cyclization step is endothermic (15.9 kJ/mol), resulting in an almost even split between the linear and cyclic tetramer products as explained by the almost isoenergetic nature of these states (5B, states i and j). Structures corresponding to states a-e can be found in Appendix Figure 5, labeled as 15-16, 19, and 21-22. Likewise, the structure for state f can be found in Appendix Figure 3, labelled as 1A, and structures corresponding to states g-j can be found in Appendix Figure 13, labeled as 17, 19-20, and 22.

Detailed reaction extent analysis is provided in the Appendix as Appendix Figures 16 – 20 and Appendix Tables 1- 14. Overall, the reaction extent analysis reveals that the growth pathways will progress to formation of the tetramer species. Interestingly, it suggests that the presence of $Na^+$ results in a higher percentage of total Si remaining in the linear tetramer configuration rather than forming the cyclic tetramer species, as in every other growth pathway. This is evidenced by the silicate system with $Na^+$ (purple path in Figure 5A) and the aluminosilicate system with $Na^+$ and Si/Al=1.

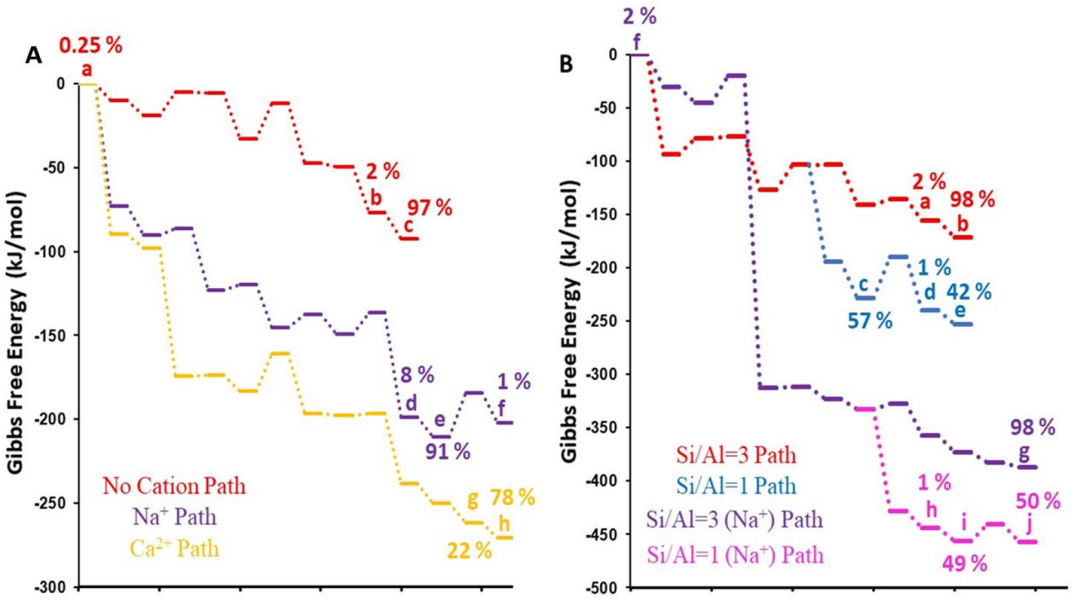


**Figure 5 Free energy reaction profiles for oligomerization of A) silicate system in the absence of cations (red) and in the presence of NaOH (purple) and $Ca(OH)_2$ (yellow), and of B) aluminosilicate system in the absence of cations with Si/Al=3 (red) and Si/Al=1 (blue) and in the presence of NaOH with Si/Al=3 (purple) and Si/Al=1 (pink). States labeled (a, b, etc.) along the pathways indicate the complexes that are found to be in highest concentration within each individual path based on reaction extent calculations. Percentages shown for each labeled state correspond to the mol % of Si in each respective complex and are color-coded to indicate the path to which they belong. The species in panel A are as follows: a - $Si(OH)_4$, b - cyclic tetramer + $H_2O$, c - cyclic tetramer, d - linear tetramer with $Na^+$ + $H_2O$, e - linear tetramer with $Na^+$, f - cyclic tetramer with $Na^+$, g - cyclic tetramer with $Ca^{2+}$ + $H_2O$ , and h - cyclic tetramer with $Ca^{2+}$. The species in panel B are as follows: a - cyclic tetramer (Si/Al=3) + $H_2O$, b - cyclic tetramer (Si/Al=3), c - linear tetramer (Si/Al=1) + $H_2O$, d - cyclic tetramer (Si/Al=1) + $H_2O$, e - cyclic tetramer (Si/Al=1), f - $Si(OH)_4$, g - cyclic tetramer with $Na^+$ (Si/Al=3), h - linear tetramer with $Na^+$ (Si/Al=1) + $H_2O$, i - linear tetramer with $Na^+$ (Si/Al=1), and j - cyclic tetramer with $Na^+$ (Si/Al=1). The growth pathways progress to convert most Si content to the tetramer species, either linear or cyclic, with the linear complexes often appearing in the media containing $Na^+$.**

### 3.9 Cation Substitution

After exploring the initial steps in zeolite formation, the focus of this work shifted to further understanding the role and atomic placement of cations in zeolites and we investigated cation substitution in zeolite crystal cells. All substitution calculations were performed on a 354-atom faujasite (FAU) crystal cell adapted from the FAU framework on the International Zeolite Association database[61]. All substitutions were made in the high-layer region of at either tetrahedrally coordinated metal sites (Si, Al) or in place of charge balancing Brønsted acid sites, for framework and extraframework substitution, respectively. We would like to note here that in the remainder of this work when we are discussing surface substitution, we are referring to a substitution occurring on the external surface of the zeolite crystal cell. Likewise, when we discuss bulk substitution, we are referring to a substitution that does not occur on the external surface of the zeolite crystal cell. Here we look at substitution of $Al^{3+}$ and $Zn^{2+}$ into the FAU crystal framework, and the substitution of $Na^{+}$, $Zn^{2+}$, and a combination of the two as extraframework cations. In addition to being regularly found in the composition of FAU zeolites[62], we chose to investigate the substitution of $Al^{3+}$ and $Na^{+}$ because of the results of the aluminosilicate oligomer growth portion of our work. It was shown that aluminosilicate oligomerization was thermodynamically preferred over pure silicate oligomerization, and in general the introduction of $Na^{+}$ to the system further increased the exothermicity of growth. In the case of $Zn^{2+}$, when investigating aluminosilicate oligomerization (in the presence of $Zn^{2+}$) it was found that growth past the trimer species was limited, which made its behavior during substitution into the crystal cell particularly interesting. In cases where the substitution of a cation into a $Si^{4+}$ site would result in a charge imbalance, the appropriate number of Brønsted acid sites ($H^{+}$) were added to bridging oxygen atoms in the framework (introduced to the system by the cation complexes). To fully

investigate the positions of these cations, we accounted for substitution both in the bulk (Figure 6, a-b) and on the surface (Figure 6, c-d) of the zeolite crystal.

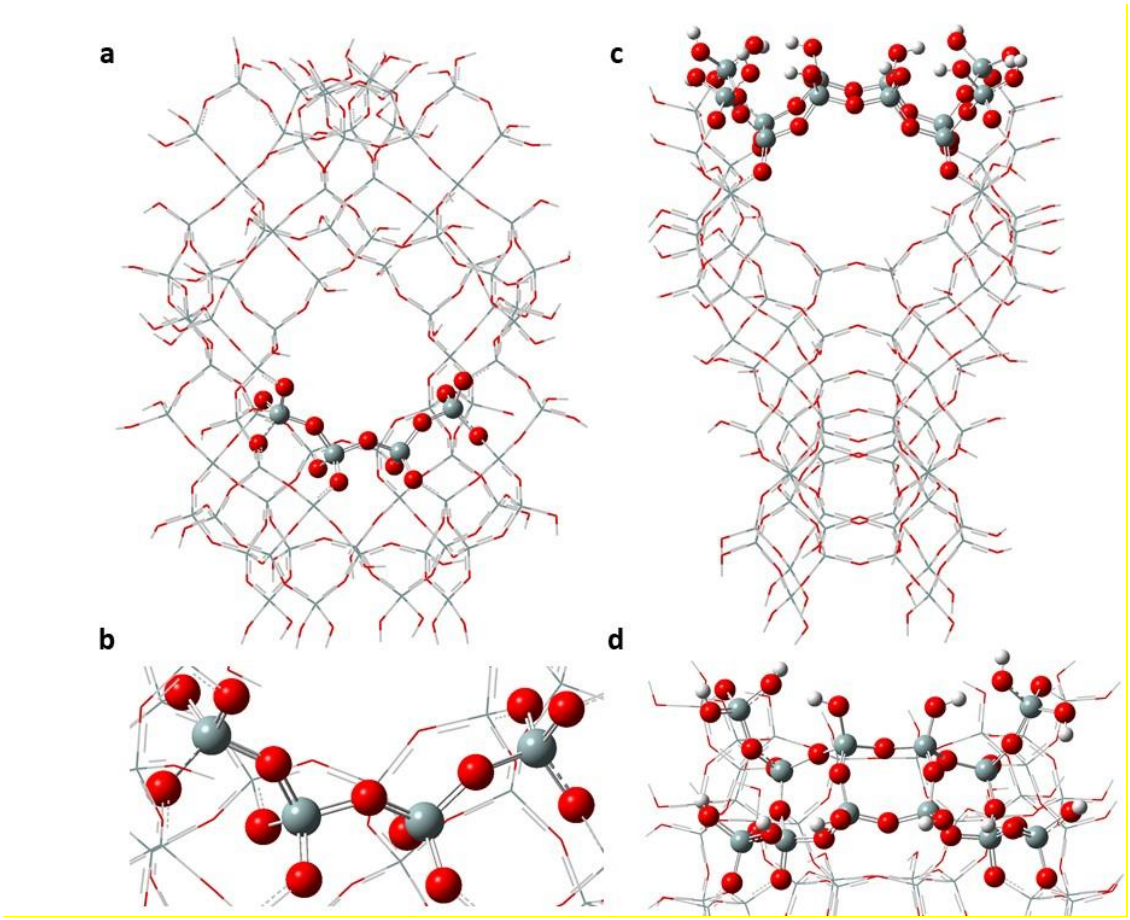


**Figure 6 Zeolite crystal cells with FAU zeolite topology. The portion of the framework displayed with ball-and- stick is the high-layer portion of the system calculated at most accurate level of theory (ab-initio). The portion of the framework displayed with bond-line is the low-layer portion of the system calculated with the lower level of theory (semiempirical). a) visualization of partitioning of high and low-layer portions of bulk system b) enhanced view of high-layer portion of bulk system c) visualization of partitioning of high and low-layer portions of surface system (includes terminating -OH groups) d) enhanced view of high-layer portion of surface system (includes terminating -OH groups).**

### 3.10 Framework Substitution

The first step taken to investigate the impact of cations on the FAU framework was to perform a substitution of either $Al^{3+}$ (in the form $Al(OH)_3(H_2O)$ as reference) or $Zn^{2+}$ (in the form $Zn(OH)_2(H_2O)_2$ as reference) in the place of a $Si^{4+}$ (producing $(Si(OH)_4$). The reaction that takes place in $Al^{3+}$ substitution is $Si_{84}O_{202}H_{68} + Al(OH)_3(H_2O) \rightarrow Si_{83}AlO_{202}H_{69} + Si(OH)_4$. Likewise, the reaction for $Zn^{2+}$ substitution is $Si_{84}O_{202}H_{68} + Zn(OH)_2(H_2O)_2 \rightarrow Si_{83}ZnO_{202}H_{70} + Si(OH)_4$. Introducing the cations into the system in this form allows the system to remain charge neutral at all times. These substitutions were made in both surface and bulk positions of the pure silicate FAU cell (Si in Table 1), aluminosilicate FAU cell (AlSi in Table 1), and zincosilicate FAU cell (ZnSi in Table 1). Table 1 displays the substitution energy in kJ/mol for substitution of cations into specific FAU cells (initial systems). As is shown in Table 1, zinc substitution in bulk positions was found to be endothermic, with Gibbs free energies of 47.2 and 38.9 kJ/mol for substitution in pure silicate bulk (Appendix Figure 21, state labeled ZnSi-Bulk) and aluminosilicate bulk (Appendix Figure 21, state labeled ZnAl- Bulk), respectively. This can be attributed to zinc's preference to be tri-coordinated, thus breaking Zn-O bonds during relaxation to achieve that preferred coordination. Though this is also seen in surface calculations (Appendix Figure 21, states labeled ZnSi-Surface, ZnAl-Surface, and 2Zn-Surface) , there is less confinement at surface sites and allows more movement for atoms that have bonds broken to reorient. In fact, $Zn^{2+}$ substitution was found to be exothermic only in surface positions. In bulk positions the $Zn^{2+}$ atom is confined to the space near the oxygen atoms to which it previously had been bonded. This suggests that $Zn^{2+}$ would not be found in the bulk, but rather would be found at sites on the surface of the of the crystal cell. Defects in the framework of the crystal cell are produced when $Zn^{2+}$ is substituted in

a tetrahedral site ($Si^{4+}$) and Zn-O are broken to achieve a tri-coordinated configuration. It would be particularly interesting to see if the presence of these defects could limit the growth of the zeolite and or inhibit interzeolite transformation (i.e. transformation of metastable FAU to stable GIS[48]). Overall, $Al^{3+}$ substitution was most exothermic, with each $Al^{3+}$ substitution being exothermic on all initial systems, both on surface and bulk positions. In bulk positions specifically, the substitution of $Al^{3+}$ was highly exothermic with $Al^{3+}$ substitution of a $Si^{4+}$ atom in the bulk aluminosilicate system most exothermic (-343.3 kJ/mol), forming the 2 Al substituted bulk framework (Appendix Figure 21, state labeled 2 Al- Bulk). The formation pathways of the above discussed substituted systems are given in Figure 7, which clearly depicts the differences in the energetics of the surface and bulk systems.

**Table 1 Gibbs free energies in kJ/mol for substitution in the framework of FAU zeolite crystal cell. Initial system refers to the zeolite structure to which substitution is being performed. The abbreviations provided in the initial system column (left) refers to the following zeolite systems: Si- silicate, AlSi- aluminosilicate, ZnSi- zincosilicate. The middle and right columns (Al and Zn) denote the cation that is being substituted in place of a Si atom. Surface and bulk designations refer to the location where the substitution is taking place. Energetics for all substitution calculations are color-coded for upmost clarity: red- endothermic, blue- exothermic, green- highly exothermic. Structures for all initial and resulting systems given in Appendix Figure 21.**

| Initial System | Al | Zn |
|---|---|---|
| Si – Surface | -57.4 | -28.1 |
| Si – Bulk | -241.2 | 47.2 |
| AlSi –Surface | -14.1 | -30.1 |
| AlSi –Bulk | -343.3 | 38.9 |
| ZnSi – Surface | -59.4 | -61.9 |
| ZnSi –Bulk | -249.5 | -- |

Endothermic
Exothermic
Highly Exothermic

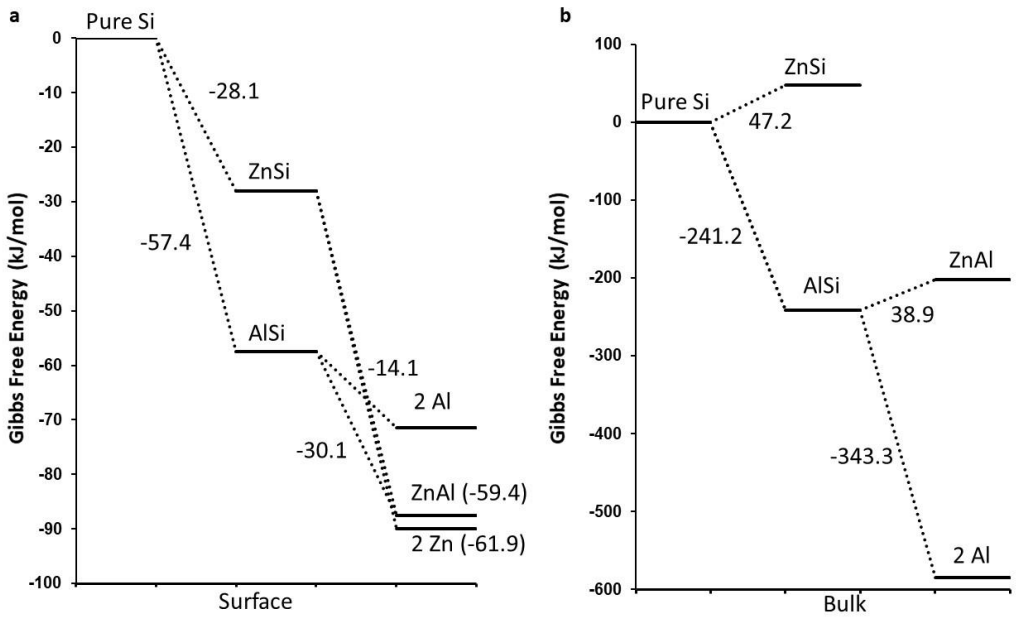


**Figure 7 Free energy reaction profiles for a) surface and b) bulk cation substitution of framework Si atoms in FAU zeolite crystal cells. States are labeled with abbreviation of system and represent the following: Pure Si- silicate, ZnSi- zincosilicate, AlSi- aluminosilicate, 2Al- 2 aluminum containing aluminosilicate, ZnAl- zincoaluminosilicate, 2Zn- 2 zinc containing zincosilicate. Structures for all states are provided in Appendix Figure 22.**

## 3.11 Extraframework Substitution

Following the investigation of cation substitution into the framework positions of these FAU zeolite systems, the substitution of cations into extraframework positions were also evaluated to fully examine the possible positions of cations in the final zeolite product. In substitution calculations performed on extraframework sites, the cations were substituted on Brønsted acid sites (replacing a proton). For each substitution of $Zn^{2+}$, two Brønsted acid sites were substituted, with $Zn^{2+}$ bridging the two oxygens where the $H^{+}$ were prior to substitution. In the case of $Na^{+}$ substitution, two $Na^{+}$ atoms were substituted on two separate Brønsted acid sites, for consistency

with the $Zn^{2+}$ substitution calculations. As is displayed in Table 2, the substitution of $Na^{+}$ onto extraframework positions were found to be highly exothermic in all cases, both in the bulk and on the surface. Consistent with what was seen in the framework $Zn^{2+}$ substitution cases, $Zn^{2+}$ substitution was found to be exothermic on the surface only. It is important to note that the zincosilicate (ZnSi) and zincoaluminosilicate (ZnAl) bulk systems would not be formed in the first place, as can be seen above in Table 1, where formation of these structures were both found to be endothermic. The formation pathways to these structures can be found in Figure 8, for both surface and bulk. These systems were included in this analysis in order to be fully comprehensive. In the case of the zincoaluminosilicate system (ZnAl in Table 2), there are three separate Brønsted acid sites which provided the unique opportunity to evaluate the substitution of a single $Na^{+}$ cation and a single $Zn^{2+}$ cation, which would be consistent with the environment present in zeolite synthesis ($Na^{+}$ cations are commonly present in zeolite synthesis, regardless of if the system contains $Zn^{2+}$). We see in this case that including $Na^{+}$ with $Zn^{2+}$ substitution the energetics become exothermic.

**Table 2 Gibbs free energies in kJ/mol for substitution on the extraframework positions of FAU zeolite crystal cell. Initial system refers to the zeolite structure to which substitution is being performed. The abbreviations provided in the initial system column (left) refers to the following zeolite systems: 2Al- 2 aluminum containing aluminosilicate, ZnSi- zincosilicate, ZnAl- zincoaluminosilicate. The middle two and right-hand columns ($Na^+$, $Zn^{2+}$, and $Na^+/Zn^{2+}$) denotes the cation that is being substituted in place of Brønsted acid sites ($H^+$) . Surface and bulk designations refer to the location where the substitution is taking place. Energetics for all substitution calculations are color-coded for upmost clarity: red- endothermic, blue- exothermic, green- highly exothermic. Structures for all initial and resulting systems given in Appendix Figure 23.**

| Initial System | $Na^+$ | $Zn^{2+}$ | $Na^+/Zn^{2+}$ |
|---|---|---|---|
| 2Al –Surface | -362.3 | -80.6 | -- |
| 2Al –Bulk | -406.9 | 77.6 | -- |
| ZnSi – Surface | -154.7 | -25.3 | -- |
| ZnSi –Bulk | -389.7 | 45.9 | -- |
| ZnAl –Surface | -327.3 | 20.2 | -332.5 |
| ZnAl –Bulk | -389.2 | 32.7 | -130.8 |

Endothermic
Exothermic
Highly Exothermic

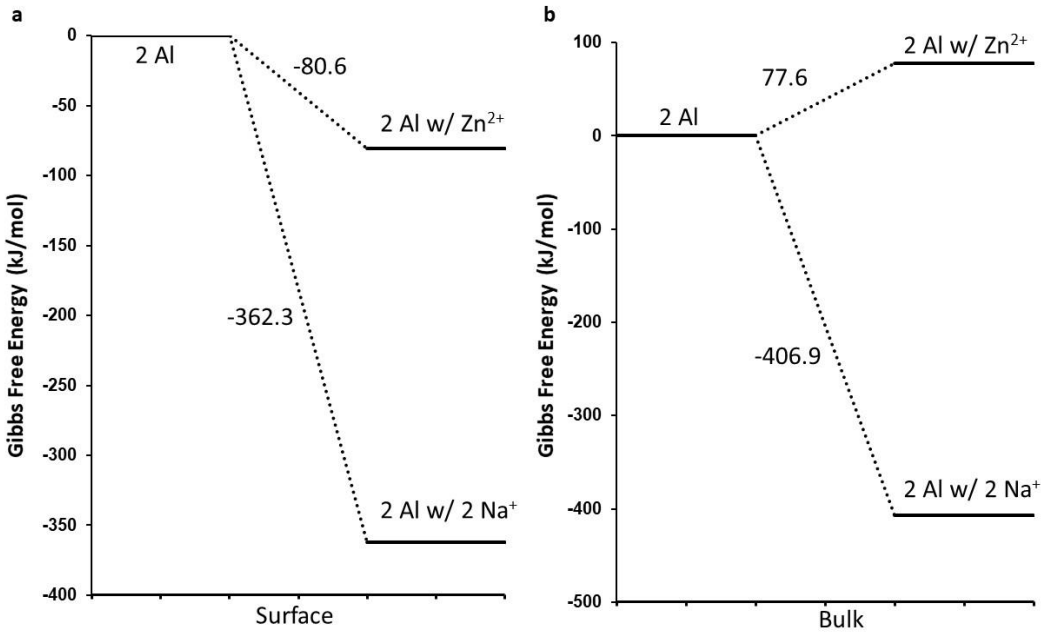


**Figure 8 Free energy reaction profiles for a) surface and b) bulk cation substitution of extraframework Brønsted acid sites ($H^+$) on FAU zeolite crystal cells. States are labeled with abbreviation of system and represent the following: 2Al- 2 aluminum containing aluminosilicate, 2Al w/ $Zn^{2+}$- 2 aluminum containing aluminosilicate with $Zn^{2+}$ extraframework cation, 2Al w/ 2 $Na^+$- 2 aluminum containing aluminosilicate with 2 $Na^+$ extraframework cations. Structures for all states are provided in Appendix Figure 24.**

## 4.0 Conclusions

Herein, we have investigated the thermodynamics of oligomerization reactions in zeolite growth for systems with varied compositions. Overall, the oligomerization of the silicate system was found to be slightly exothermic, whereas the aluminosilicate system was found to be significantly more exothermic, with the presence of aluminum increasing the exothermicity of oligomerization. We found that in aluminosilicate complexes, $H_2O$ dissociation on the complex is energetically preferred over $H_2O$ desorption, which may result in the formation of Brønsted acid sites on bridging oxygens (Si-O-Al). This suggests that Brønsted acid sites, responsible for zeolite acidity, may be first introduced during the early stages of growth as an intermediate species which then could participate in ion exchange (in the presence of cations). The thermodynamics of silicate complexes growth were also evaluated in the presence of $Na^+$, $Ca^{2+}$, and $Zn^{2+}$. All three cations increase the exothermicity of silicate oligomerization, with $Ca^{2+}$ exhibiting the most exothermic path, which is particularly interesting as $Ca^{2+}$ is often found in naturally occurring zeolites. Furthermore, introducing divalent cations ($Ca^{2+}$ and $Zn^{2+}$) into the silicate system provided an alternative growth pathway due to their divalent nature, acting as a bridge between two Si atoms by the formation of OCaO or OZnO bonds. Moreover, to elucidate the cation effect in aluminosilicate growth, we considered the presence of $Na^+$ and $Zn^{2+}$, which both increased the exothermicity of the reaction pathways similarly to case of silicates. In all aluminosilicate systems, the tetramer product with Si/Al ratio of  was found to be energetically preferred over the tetramer product with Si/Al ratio of 3. Cyclic structure formation was evaluated for each (alumino)silicate complex (dimer, trimer, etc.). Apart from the dimer species, cyclization was found to be favorable for all silicate and aluminosilicate complexes both in the presence and absence of cations. Reaction

extent analysis suggests that all growth pathways will progress to convert most Si introduced as a reactant to the tetramer species, either linear or cyclic, with the linear complexes appearing in the media containing $Na^+$. Overall, this portion of our computational work reveals the oligomerization thermodynamics during early stages of zeolite growth and the impact of cations on altering the speciation of preferred complexes and unravels the complexity of reaction steps taking place during early nucleation stages of zeolite growth, which can further aid the control of materials synthesis. With the early stages of zeolite growth being practically infeasible to track with experiments, this computational work demonstrates the detailed thermodynamics of oligomerization and how speciation changes in the presence of cations.

In addition to the investigation of initial zeolite oligomerization steps, we also explored the role and position of cations in zeolite cells by performing cation substitutions over a variety of zeolite crystal systems. Substitution was performed in both surface and bulk sites, and cations were substituted as both framework and extraframework cations. $Al^{3+}$ was found to be the most energetically favorable cation for framework substitution for all systems, with $Zn^{2+}$ framework substitution only being exothermic on the surface due to a preferred tri-coordination. $Na^+$ and $Zn^{2+}$ were substituted as extraframework cations on Brønsted acid sites on both bulk and surface positions. The substitution of $Na^+$ was found to be highly exothermic in all cases, whereas substitution of $Zn^{2+}$ was found to be exothermic only on surface sites which is consistent with framework substitution of $Zn^{2+}$.

Looking ahead, computational efforts should focus on larger oligomers and their overall impact on zeolite structure. For instance, although at the conditions of interest we revealed a polymeric behavior of oligomerization, it is unclear if oligomer growth stops at larger complexes (of specific size) or continues this polymeric behavior. Oligomers stabilized at specific sizes can

in turn act as building blocks in zeolite growth. Theory and experiments should be tightly coupled together to understand if highly stable oligomers formed at the early growth stages act as building units for zeolites or as spectator species. Additionally, further investigations should be made into substitution of cations into other compositions and topologies of zeolite crystal cells. The potential to find ways to modify zeolite crystal composition to direct growth towards or away from certain products has an abundance of possible applications across several fields. Again, working closely with experimental investigators to approach these problems with a wholistic approach will be invaluable to the fields of zeolite synthesis and applications.

# Appendix Supplementary Information

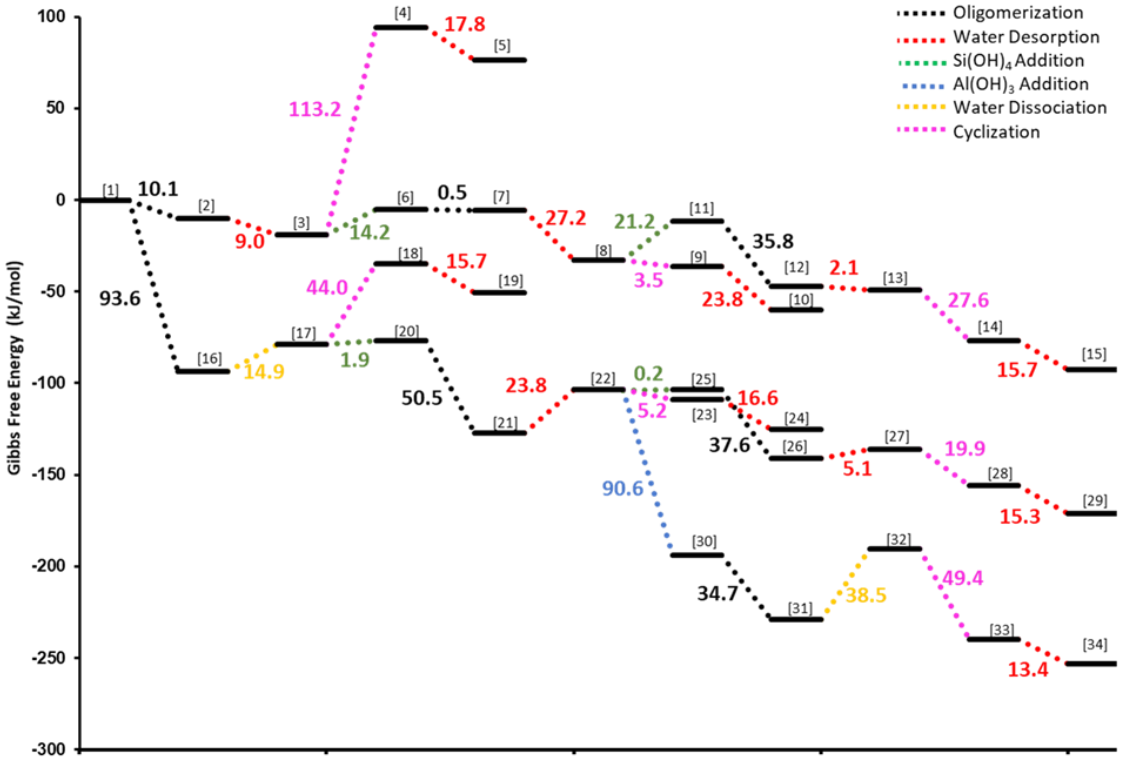


**Appendix Figure 1 Free energy reaction profiles for oligomerization of silicate and aluminosilicate systems, as shown in Figure 1 of the manuscript. The structure for each numbered state is shown in Appendix Figure 3.**

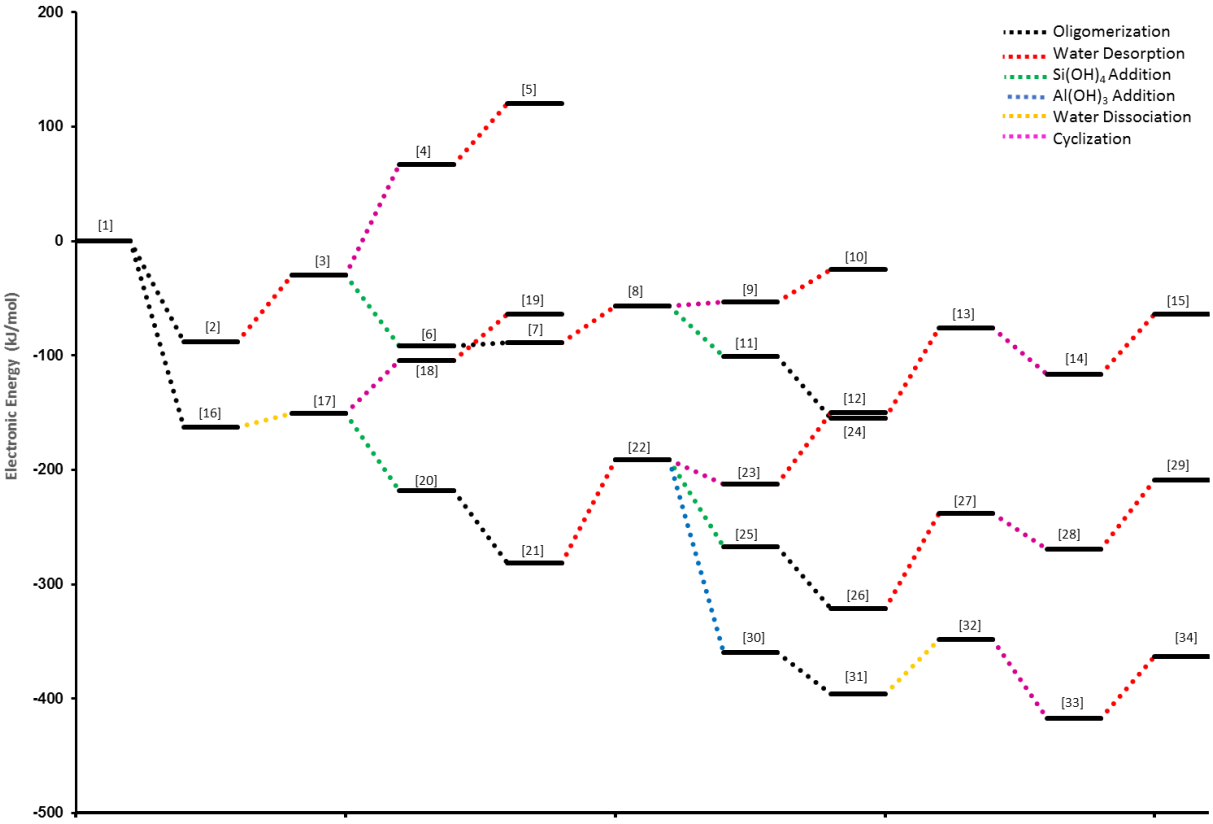


**Appendix Figure 2 Electronic energy reaction profiles for oligomerization of silicate and aluminosilicate systems, corresponding to Figure 1 of the manuscript. The structure for each numbered state is shown in Appendix Figure 3.**

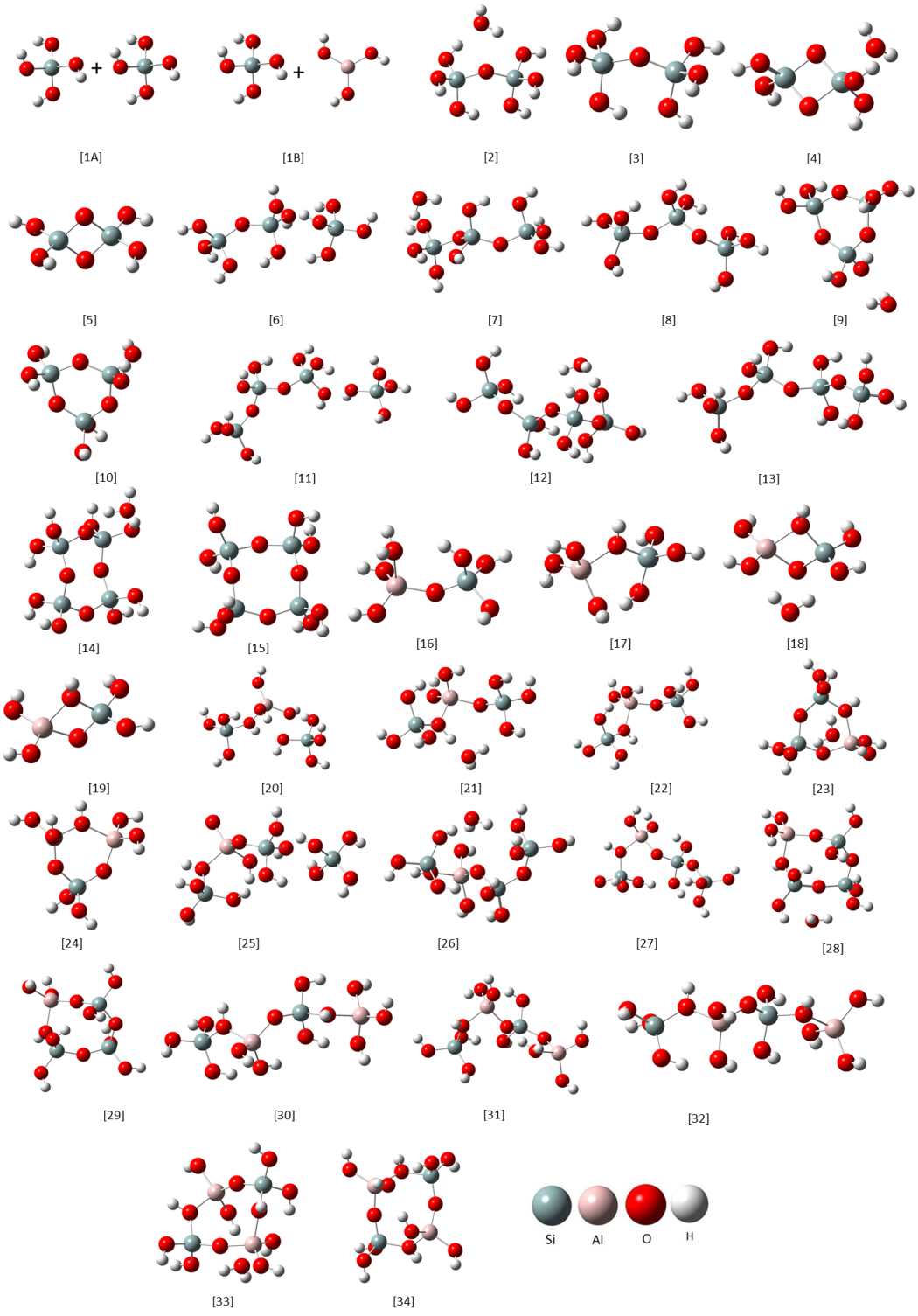


**Appendix Figure 3 Structures for each numbered state on the oligomerization pathway of silicate and aluminosilicate systems shown in Appendix Figures 1 and 2. Structures 1A and 1B are the initial reactants for the silicate and aluminosilicate systems, Si(OH)4 + Si(OH)4 and $Si(OH)_4$ + $Al(OH)_3$, respectively.**

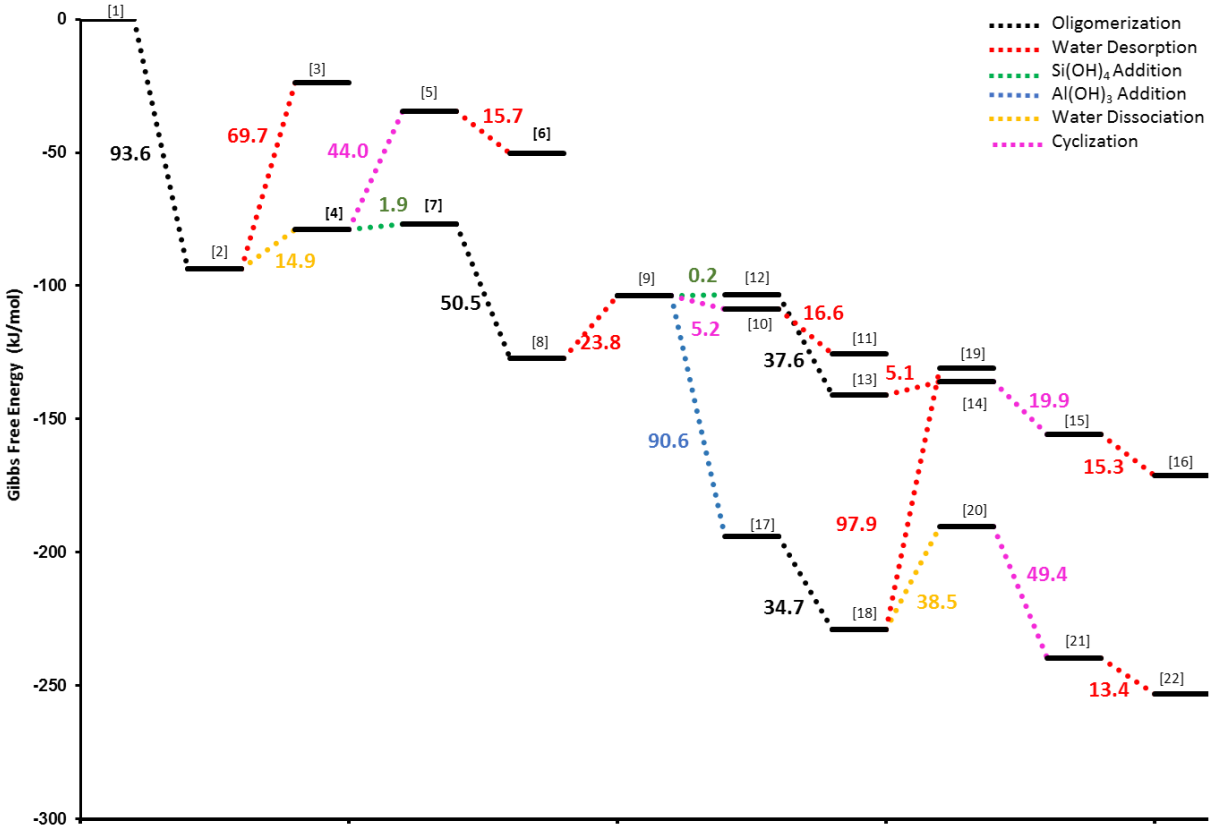


**Appendix Figure 4 Free energy reaction profiles for oligomerization of aluminosilicate system, as shown in Figure 2 of the manuscript. The structures for each numbered state are shown in Appendix Figure 5.**

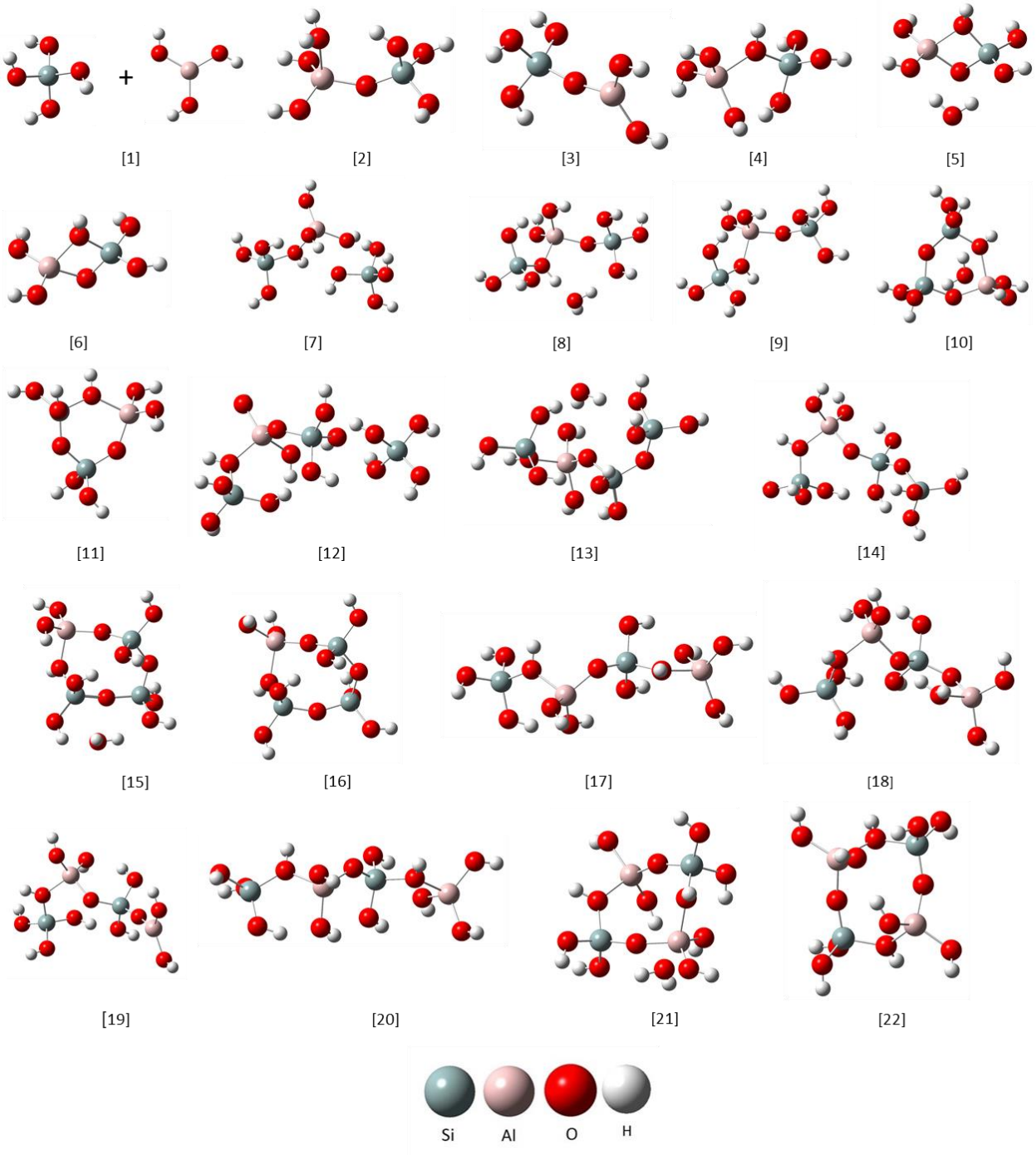


**Appendix Figure 5 Structures for each numbered state on the oligomerization pathway of aluminosilicate system, as given in Appendix Figure 4.**

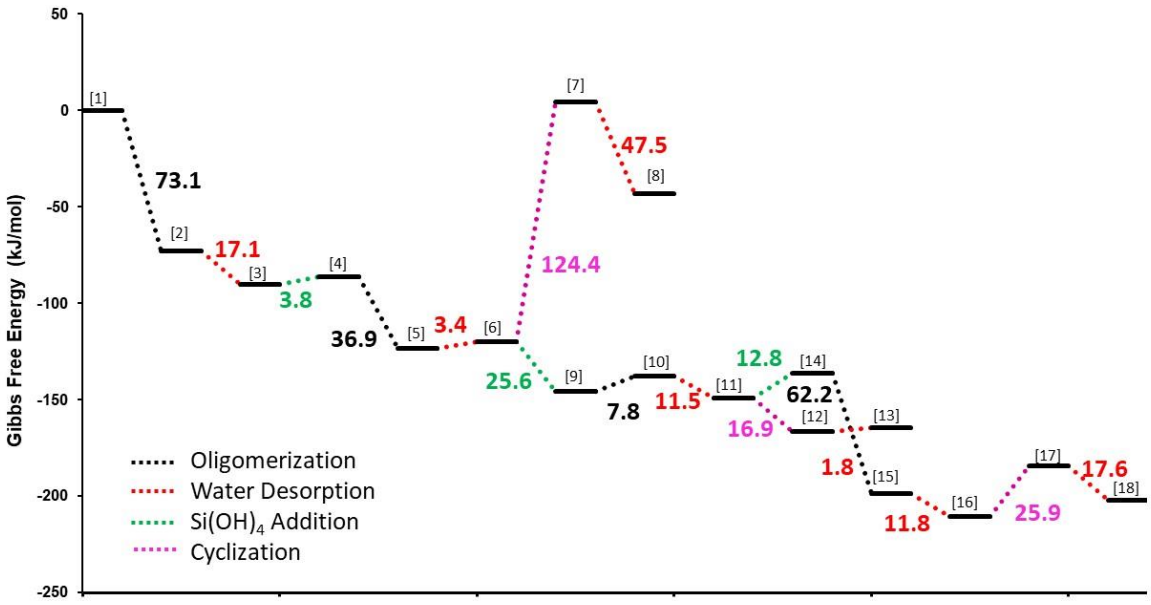


**Appendix Figure 6 Free energy reaction profiles for oligomerization of silicate system in the presence of NaOH, as shown in Figure 3 of the manuscript. The numbered states are used as a guide for the structures presented in Appendix Figures 7.**

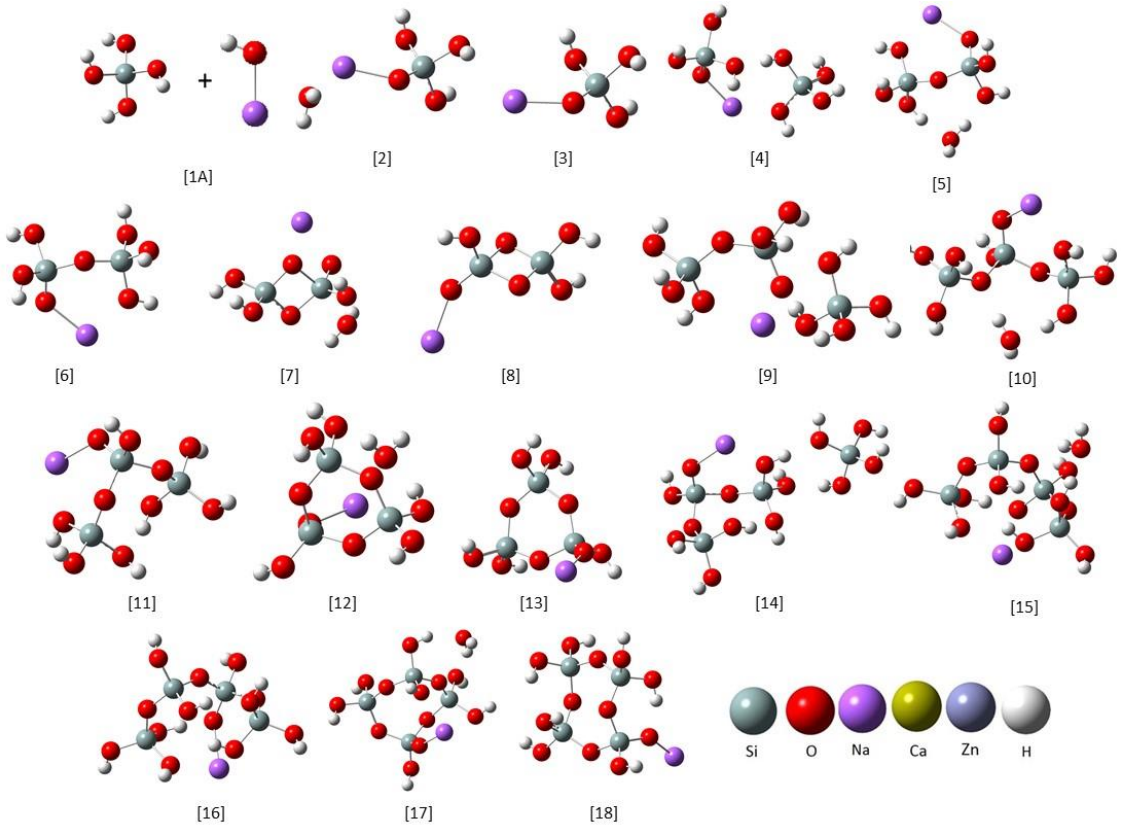


**Appendix Figure 7 Structures for each numbered state on the oligomerization pathway of silicate system in the presence of NaOH, as given in Appendix Figure 6.**

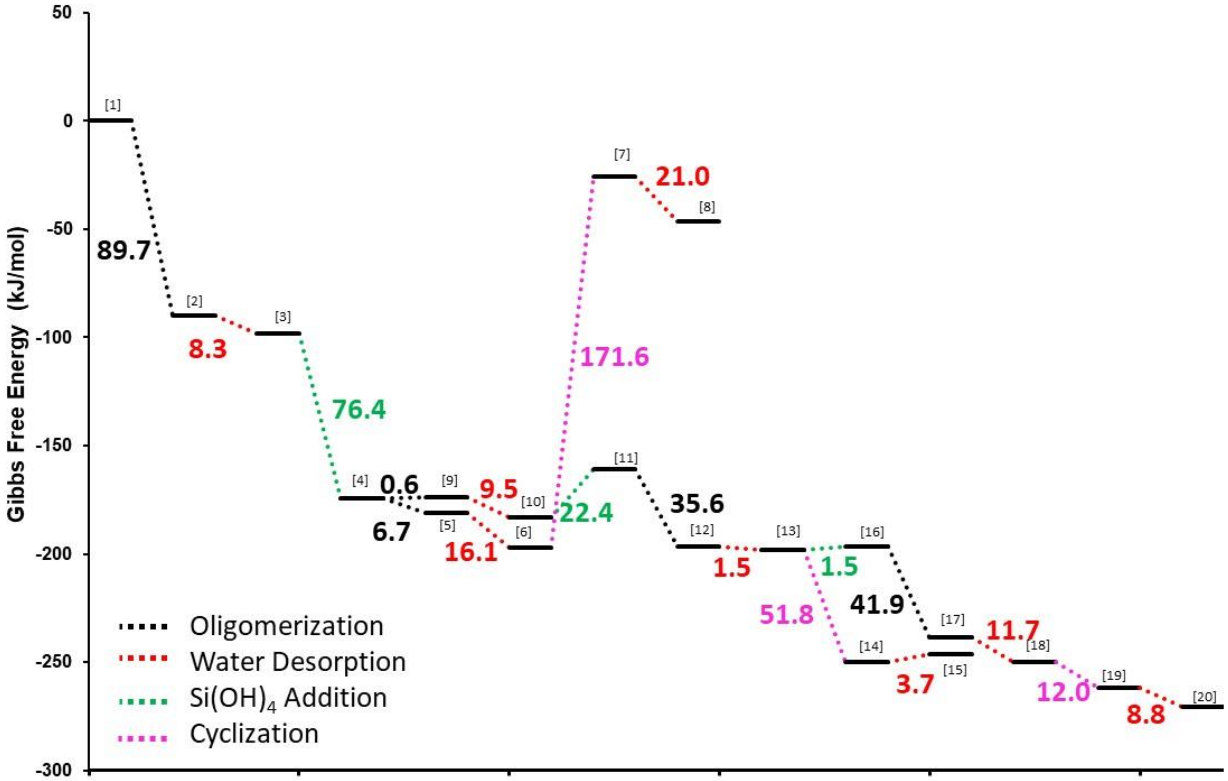


**Appendix Figure 8 Free energy reaction profiles for oligomerization of silicate system in the presence of Ca(OH)2, as shown in Figure 3 of the manuscript. The numbered states are used as a guide for the structures presented in Appendix Figures 9.**

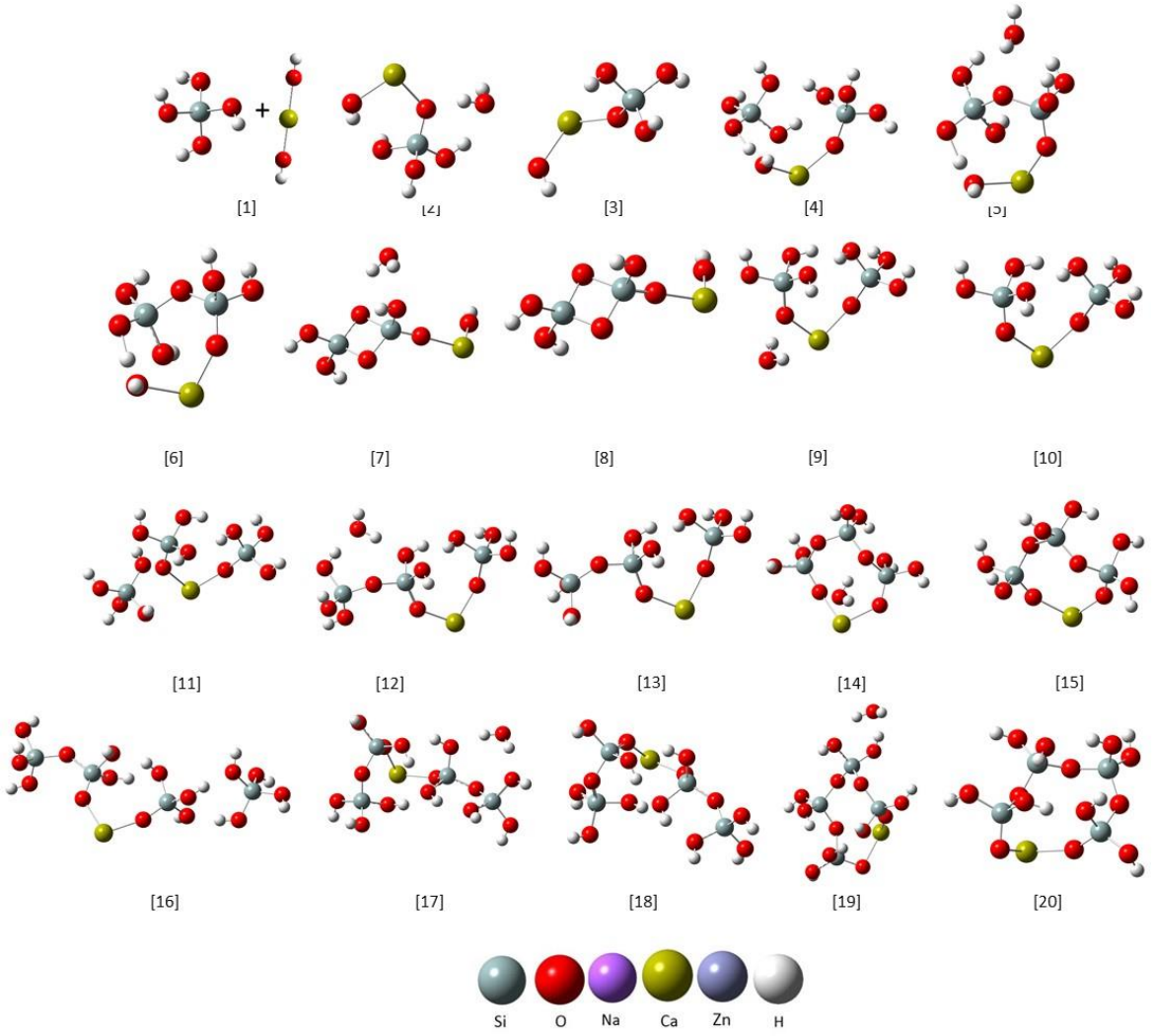


**Appendix Figure 9 Structures for each numbered state on the oligomerization pathway of silicate system in the presence of Ca(OH)2, as given in Appendix Figure 8.**

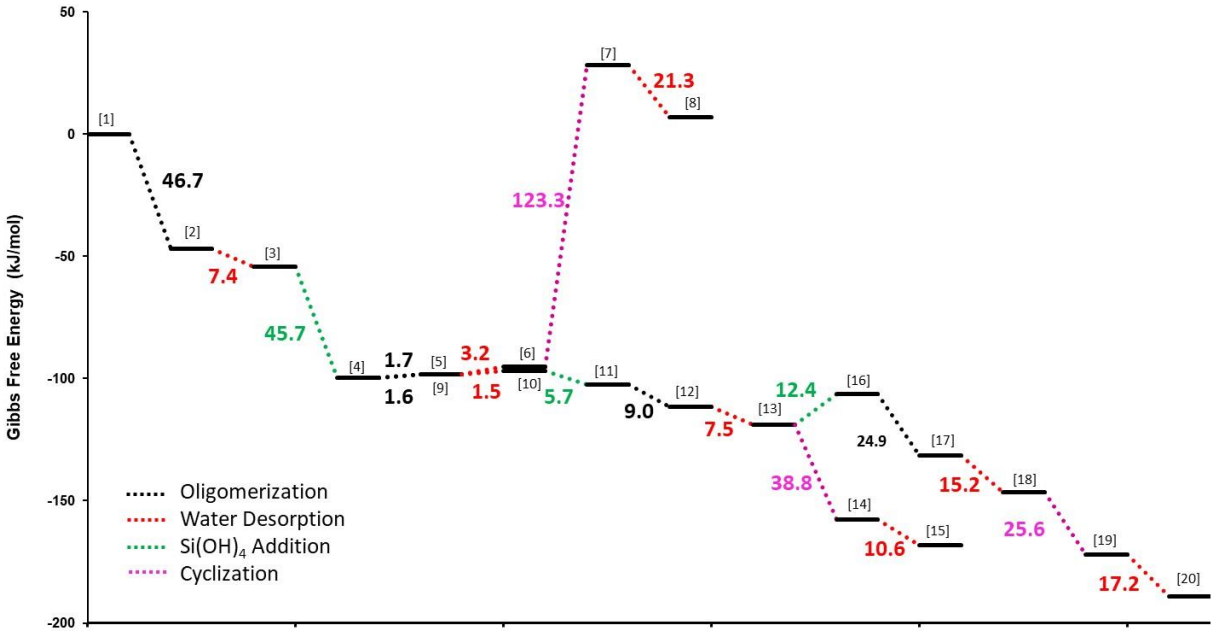


**Appendix Figure 10 Free energy reaction profiles for oligomerization of silicate system in the presence of Zn(OH)2, as shown in Figure 3 of the manuscript. The numbered states are used as a guide for the structures presented in Appendix Figures 11.**

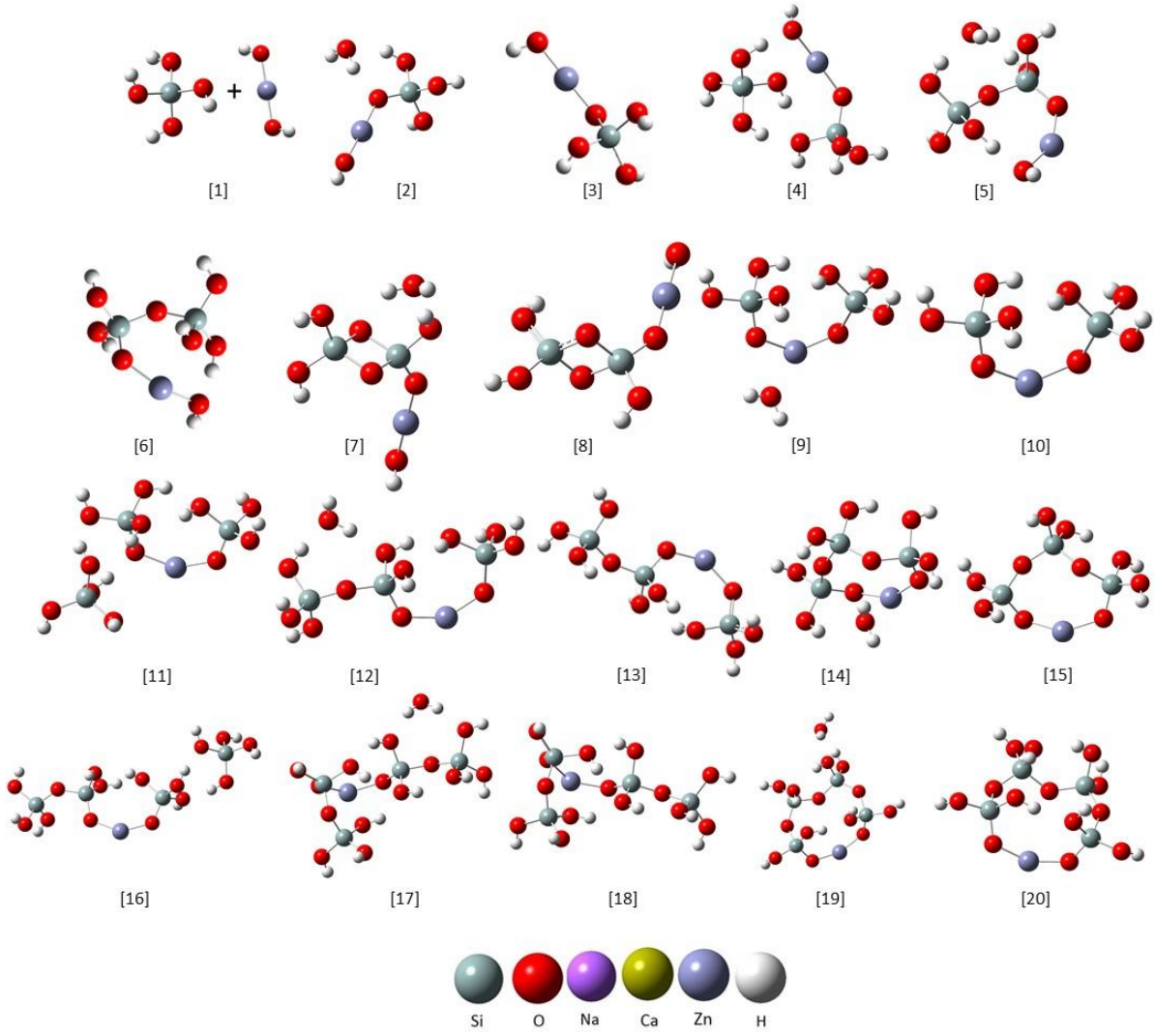


**Appendix Figure 11 Structures for each numbered state on the oligomerization pathway of silicate system in the presence of Zn(OH)2, as given in Appendix Figure 10.**

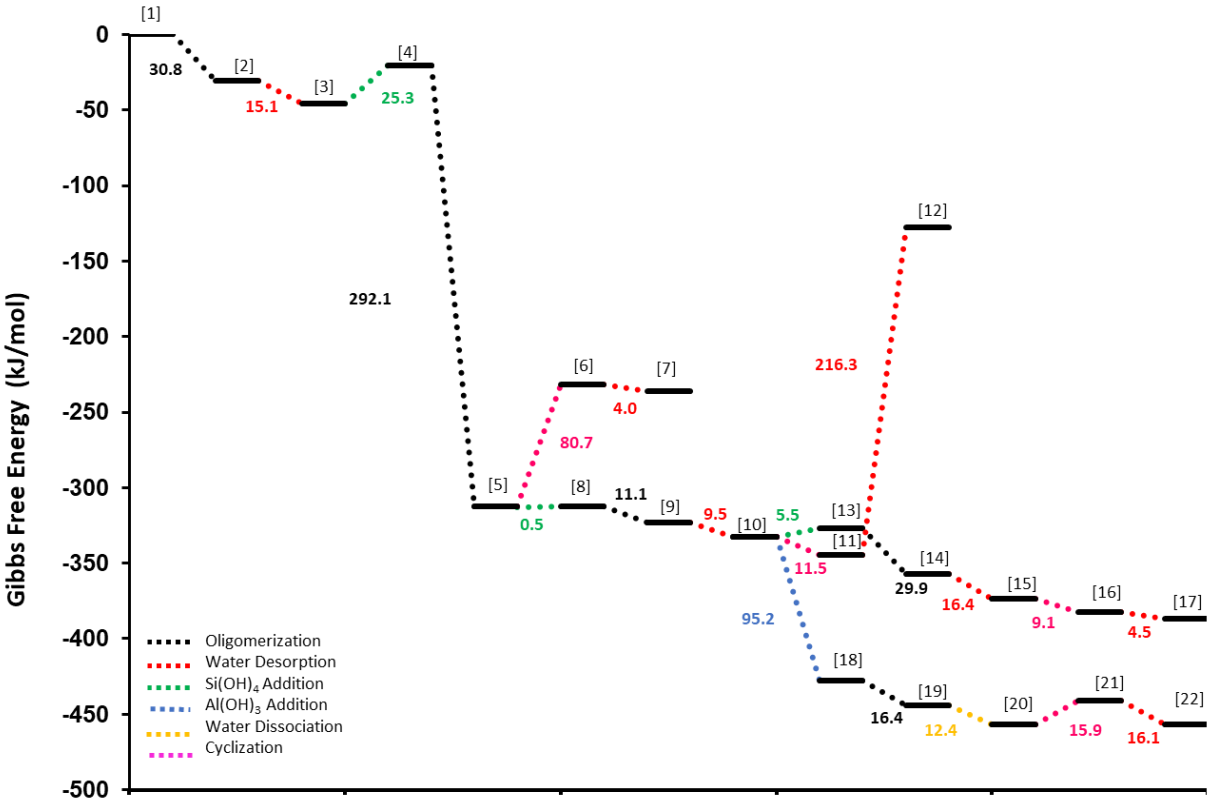


**Appendix Figure 12 Free energy reaction profiles for oligomerization of aluminosilicate system in the presence of NaOH, as shown in Figure 4 of the manuscript. The numbered states are used as a guide for the structures presented in Appendix Figure 13.**

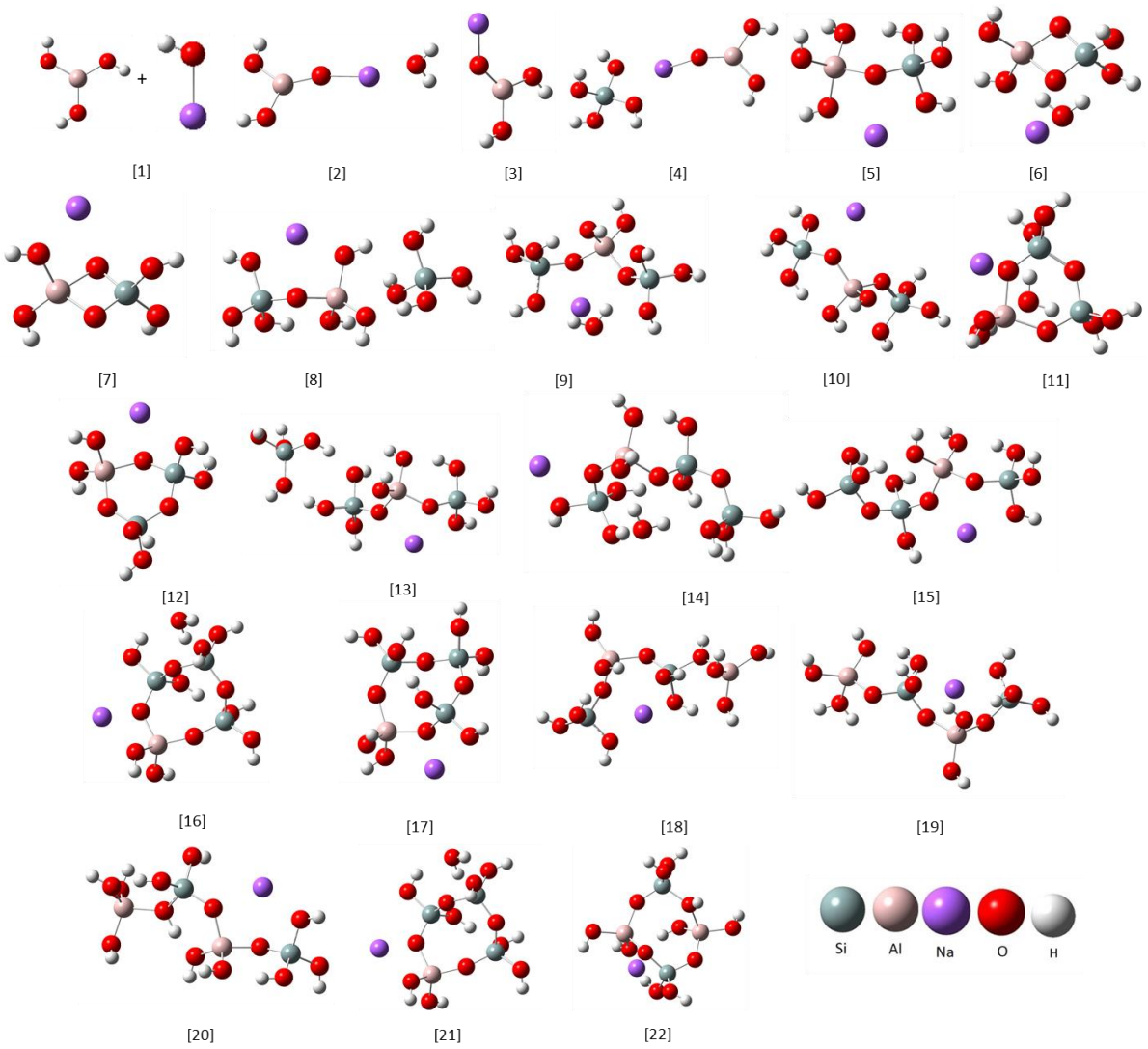


**Appendix Figure 13 Structures for each numbered state on the oligomerization pathway of aluminosilicate system in the presence of NaOH, as given in Appendix Figure 12.**

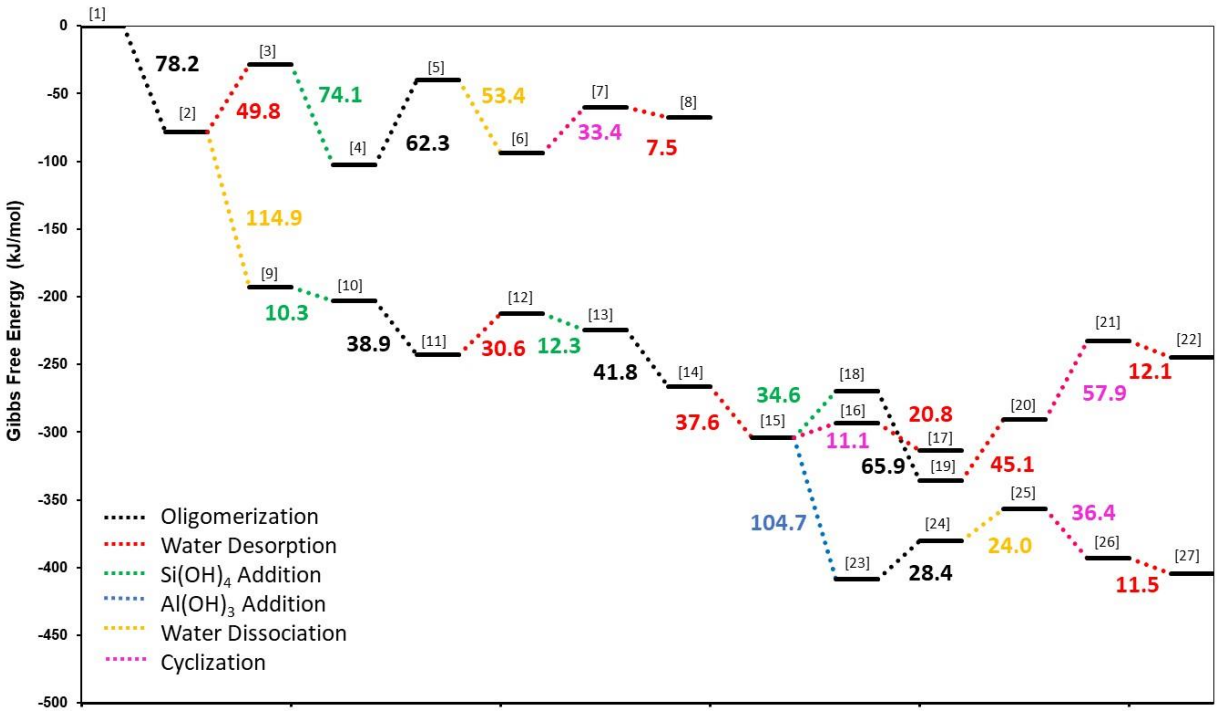


**Appendix Figure 14 Free energy reaction profiles for oligomerization of aluminosilicate system in the presence of Zn(OH)2, as shown in Figure 4 of the manuscript. The numbered states are used as a guide for the structures presented in Appendix Figure 15.**

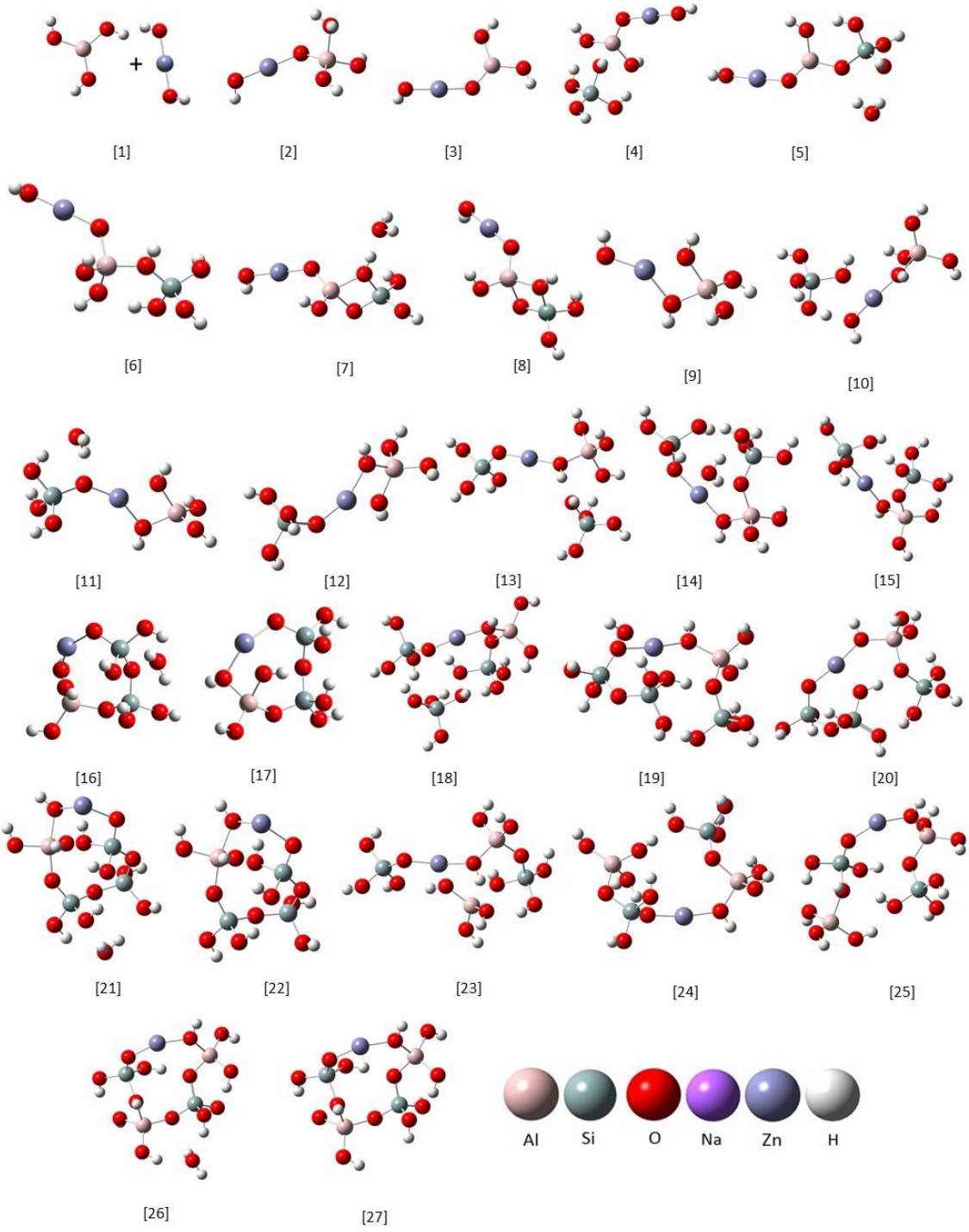


**Appendix Figure 15 Structures for each numbered state on the oligomerization pathway of aluminosilicate system in the presence of Zn(OH)2, as given in Appendix Figure 14.**

In order to determine the prominent species along a given pathway, an analysis on the reaction extent was performed based on the reported Gibbs free energies. The Gibbs free energy for each reaction step was used to determine the equilibrium constant of that reaction at 373 K. The lsqnonlin solver in Matlab was used to solve a set of non-linear equations (one per each reaction step) using the calculated equilibrium constants and designating an initial concentration of reactant species. Each pathway was evaluated individually, i.e., reaction extent of silicate system was calculated independently of reaction extent of silicate in the presence of NaOH.

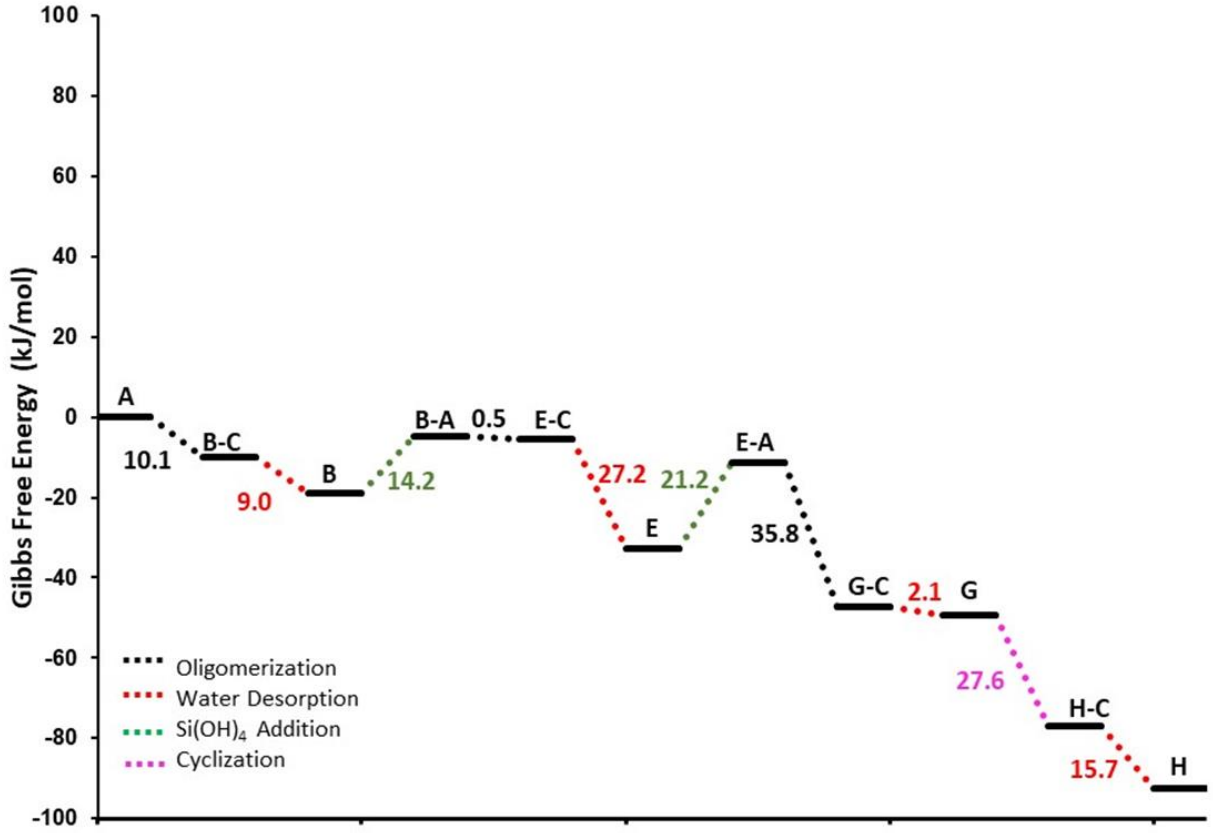


**Appendix Figure 16 Free energy reaction profile for oligomerization of the silicate system. The alphabetically labeled states are used as a guide for the reaction extent data presented in Appendix Tables 1 and 2. The initial concentration of Si(OH)4 was 4 mol.**

**Appendix Table 1 Reaction extent data for each step in the oligomerization of the silicate system up to formation of the cyclic trimer. Reaction species labeled A-H according to Appendix Figure 16.**

| Path to Tetramer | Reaction | Extent of Reaction (ξ) |
|---|---|---|
| 1 | 2 A → B-C | 1.00 |
| 2 | B-C → B + C | 1.00 |
| 3 | B +A → B-A | 1.00 |
| 4 | B-A → E-C | 1.00 |
| 5 | E-C → E + C | 1.00 |
| 6 | E + A → E-A | 1.00 |
| 7 | E-A → G-C | 1.00 |
| 8 | G-C → G + C | 1.00 |
| 9 | G → H-C | 1.00 |
| 10 | H-C → H + C | 0.97 |

**Appendix Table 2 Final number of moles, molar Si content, and total Si % of each species along the oligomerization pathway of the silicate system. Species designated A-H according to Appendix Figure 16.**

| | Species | $n_{final}$ | Si Content | Total Si % |
|---|---|---|---|---|
| A | Si(OH)4 | 0.01 | 0.01 | 0.25 |
| B | Si(OH)3-O-Si(OH)3 | 0.00 | 0.00 | 0.00 |
| C | H2O | 3.96 | 0.00 | 0.00 |
| E | Si(OH)3-O-Si(OH)2-O-Si(OH)3 | 0.00 | 0.00 | 0.00 |
| G | Si(OH)3-O-Si(OH)2-O-Si(OH)2-O-Si(OH)3 | 0.00 | 0.00 | 0.00 |
| H | OSi(OH)2-O-Si(OH)2-O-Si(OH)2-O-Si(OH)2 | 0.97 | 3.88 | 97.00 |
| B-C | Si(OH)3-O-Si(OH)3--H2O | 0.00 | 0.00 | 0.00 |
| B-A | Si(OH)3-O-Si(OH)3 -- Si(OH)4 | 0.00 | 0.00 | 0.00 |
| E-C | Si(OH)3-O-Si(OH)2-O-Si(OH)3--H2O | 0.00 | 0.00 | 0.00 |
| E-A | Si(OH)3-O-Si(OH)2-O-Si(OH)3 -- Si(OH)4 | 0.00 | 0.00 | 0.00 |
| G-C | Si(OH)3-O-Si(OH)2-O-Si(OH)2-O-Si(OH)3--H2O | 0.00 | 0.00 | 0.00 |
| H-C | OSi(OH)2-O-Si(OH)2-O-Si(OH)2-O-Si(OH)2--H2O | 0.02 | 0.08 | 2.00 |

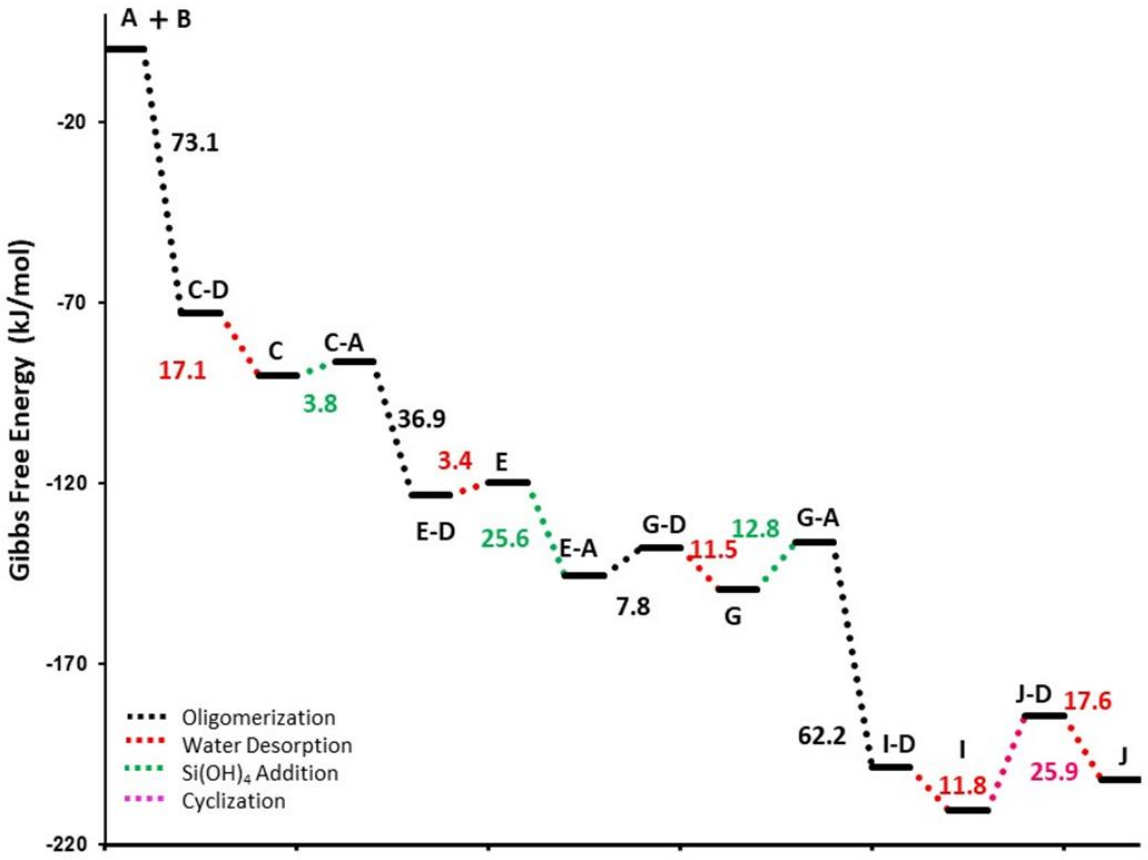


**Appendix Figure 17 Free energy reaction profile for oligomerization of silicate system in the presence of NaOH. The alphabetically labeled states are used as a guide for the reaction extent data presented in Appendix Tables 3 and 4. The initial concentrations of Si(OH)4 and NaOH were 4 mols and 1 mol, respectively.**

**Appendix Table 3 Reaction extent data for each step in the oligomerization of the silicate system in the presence of NaOH up to formation of the cyclic trimer. Reaction species labeled A-J according to Appendix Figure 17.**

| Path to Tetramer | Reaction | Extent of Reaction (ξ) |
|---|---|---|
| 1 | A + B → C-D | 1.00 |
| 2 | C-D → C + D | 1.00 |
| 3 | C + A → C-A | 1.00 |
| 4 | C-A → E-D | 1.00 |
| 5 | E-D → E + D | 1.00 |
| 6 | E + A → E-A | 1.00 |
| 7 | E-A → G-D | 1.00 |
| 8 | G-D → G + D | 1.00 |
| 9 | G + A → G-A | 1.00 |
| 10 | G-A → I-D | 1.00 |
| 11 | I-D → I + D | 0.92 |
| 12 | I → J-D | 0.02 |
| 13 | J-D → J + D | 0.01 |

**Appendix Table 4 Number of final moles, molar Si and Na content, and total Si % and Na % of each species along the oligomerization pathway of the silicate system in the presence of NaOH. Species designated A-J according to Appendix Figure 17.**

| | Species | $n_{final}$ | Si Content | Total Si % | Na Content | Total Na % |
|---|---|---|---|---|---|---|
| A | Si(OH)4 | 0.00 | 0.00 | 0.0 | 0.00 | 0.0 |
| B | NaOH | 0.00 | 0.00 | 0.0 | 0.00 | 0.0 |
| C | Si(OH)3ONa | 0.00 | 0.00 | 0.0 | 0.00 | 0.0 |
| D | H2O | 3.94 | 0.00 | 0.0 | 0.00 | 0.0 |
| E | Si(OH)3-O-Si(OH)2ONa | 0.00 | 0.00 | 0.0 | 0.00 | 0.0 |
| G | Si(OH)3-O-Si(OH)ONa-O-Si(OH)3 | 0.00 | 0.00 | 0.0 | 0.00 | 0.0 |
| I | Si(OH)3-O-Si(OH)ONa-O-Si(OH)2-O-Si(OH)3 | 0.91 | 3.64 | 91.0 | 0.91 | 91.0 |
| J | OSi(OH)2-O-Si(OH)ONa-O-Si(OH)2-O-Si(OH)2 | 0.01 | 0.04 | 1.0 | 0.01 | 1.0 |
| C-D | Si(OH)3ONa--H2O | 0.00 | 0.00 | 0.0 | 0.00 | 0.0 |
| C-A | Si(OH)3ONa -- Si(OH)4 | 0.00 | 0.00 | 0.0 | 0.00 | 0.0 |
| E-D | Si(OH)3-O-Si(OH)2ONa--H2O | 0.00 | 0.00 | 0.0 | 0.00 | 0.0 |
| E-A | Si(OH)3-O-Si(OH)2ONa-- Si(OH)4 | 0.00 | 0.00 | 0.0 | 0.00 | 0.0 |
| G-D | Si(OH)3-O-Si(OH)ONa-O-Si(OH)3--H2O | 0.00 | 0.00 | 0.0 | 0.00 | 0.0 |
| G-A | Si(OH)3-O-Si(OH)ONa-O-Si(OH)3 -- Si(OH)4 | 0.00 | 0.00 | 0.0 | 0.00 | 0.0 |
| I-D | Si(OH)3-O-Si(OH)ONa-O-Si(OH)2-O-Si(OH)3--H2O | 0.08 | 0.32 | 8.0 | 0.08 | 8.0 |
| J-D | OSi(OH)2-O-Si(OH)ONa-O-Si(OH)2-O-Si(OH)2--H2O | 0.00 | 0.00 | 0.0 | 0.00 | 0.0 |

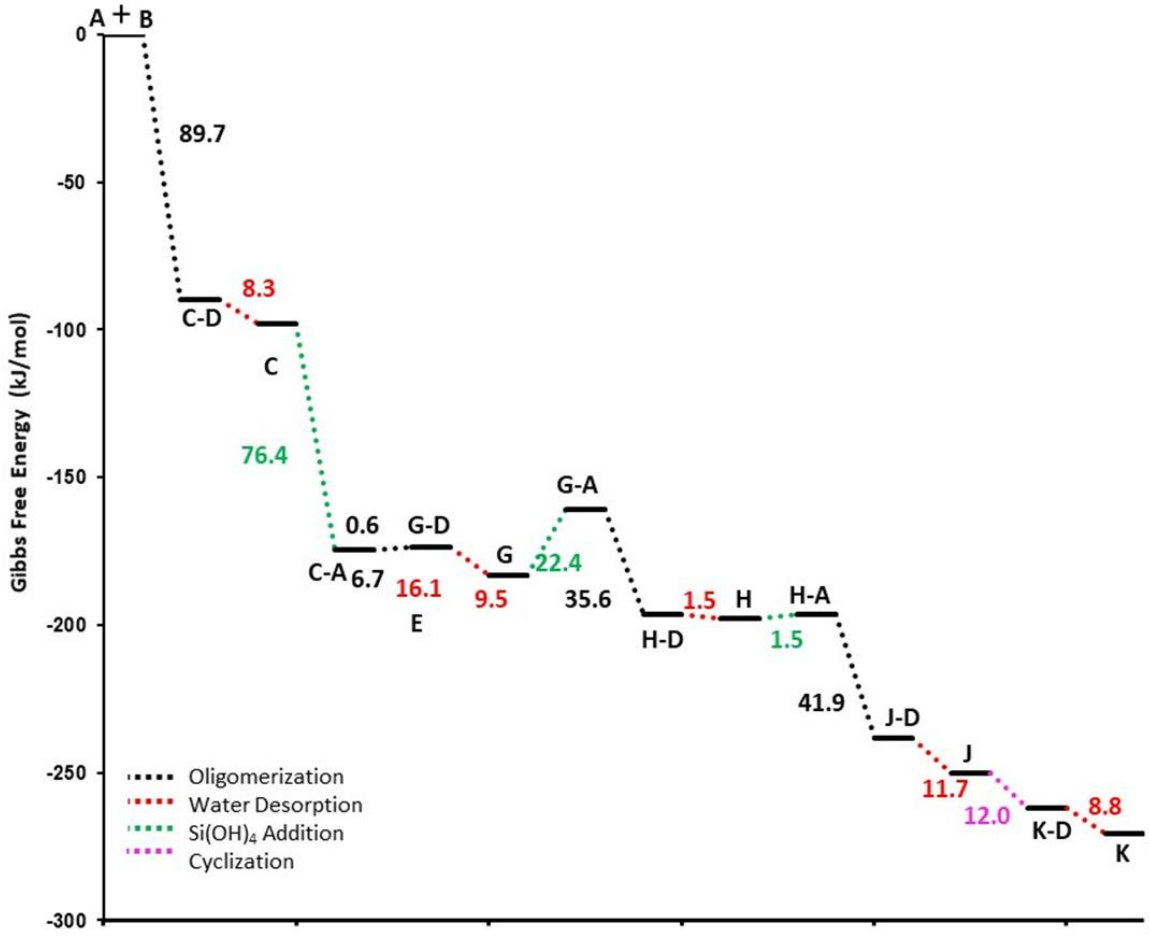


**Appendix Figure 18 Free energy reaction profile for oligomerization of silicate system in the presence of Ca(OH)2. The alphabetically labeled states are used as a guide for the reaction extent data presented in Appendix Tables 5 and 6. The initial concentrations of Si and Ca were 4 mols and 1 mol, respectively.**

**Appendix Table 5 Reaction extent data for each step in the oligomerization of the silicate system in the presence of Ca(OH)2 up to formation of the cyclic trimer. Reaction species labeled A-K according to Appendix Figure 18.**

| Path to Tetramer | Reaction | Extent of Reaction (ξ) |
|---|---|---|
| 1 | A + B → C-D | 1.00 |
| 2 | C-D → C+ D | 1.00 |
| 3 | C + A → C-A | 1.00 |
| 4 | C-A → G-D | 1.00 |
| 5 | G-D → G + D | 1.00 |
| 6 | G + A → G-A | 1.00 |
| 7 | G-A → H-D | 1.00 |
| 8 | H-D → H + D | 1.00 |
| 9 | H + A → H-A | 1.00 |
| 10 | H-A → J-D | 1.00 |
| 11 | J-D → J + D | 1.00 |
| 12 | J → K-D | 1.00 |
| 13 | K-D → K + D | 0.78 |

**Appendix Table 6 Number of final moles, molar Si and Ca content, and total Si % and Ca % of each species along the oligomerization pathway of the silicate system in the presence of Ca(OH)2. Species designated A-K according to Appendix Figure 18.**

| | Species | $n_{final}$ | Si Content | Total Si % | Ca Content | Total Ca % |
|---|---|---|---|---|---|---|
| A | Si(OH)4 | 0.00 | 0 | 0.0 | 0 | 0.0 |
| B | Ca(OH)2 | 0.00 | 0 | 0.0 | 0 | 0.0 |
| C | Si(OH)3OCaOH | 0.00 | 0 | 0.0 | 0 | 0.0 |
| D | H2O | 4.78 | 0 | 0.0 | 0 | 0.0 |
| G | Si(OH)3-OCaO-Si(OH)3 | 0.00 | 0 | 0.0 | 0 | 0.0 |
| H | Si(OH)3-OCaO-Si(OH)2-O-Si(OH)3 | 0.00 | 0 | 0.0 | 0 | 0.0 |
| J | Si(OH)3-O-Si(OH)2-OCaO-Si(OH)2-O-Si(OH)3 | 0.00 | 0 | 0.0 | 0 | 0.0 |
| K | OSi(OH)2-O-Si(OH)2-OCaO-Si(OH)2-O-Si(OH)2 | 0.78 | 3.12 | 78.0 | 0.78 | 78.0 |
| C-D | Si(OH)3OCaOH--H2O | 0.00 | 0 | 0.0 | 0 | 0.0 |
| C-A | Si(OH)3OCaOH -- Si(OH)4 | 0.00 | 0 | 0.0 | 0 | 0.0 |
| G-D | Si(OH)3-OCaO-Si(OH)3--H2O | 0.00 | 0 | 0.0 | 0 | 0.0 |
| G-A | Si(OH)3-OCaO-Si(OH)3-- Si(OH)4 | 0.00 | 0 | 0.0 | 0 | 0.0 |
| H-D | Si(OH)3-OCaO-Si(OH)2-O-Si(OH)3--H2O | 0.00 | 0 | 0.0 | 0 | 0.0 |
| H-A | Si(OH)3-OCaO-Si(OH)2-O-Si(OH)3 -- Si(OH)4 | 0.00 | 0 | 0.0 | 0 | 0.0 |
| J-D | Si(OH)3-O-Si(OH)2-OCaO-Si(OH)2-O-Si(OH)3--H2O | 0.00 | 0 | 0.0 | 0 | 0.0 |
| K-D | OSi(OH)2-O-Si(OH)2-OCaO-Si(OH)2-O-Si(OH)2--H2O | 0.22 | 0.88 | 22.0 | 0.22 | 22.0 |

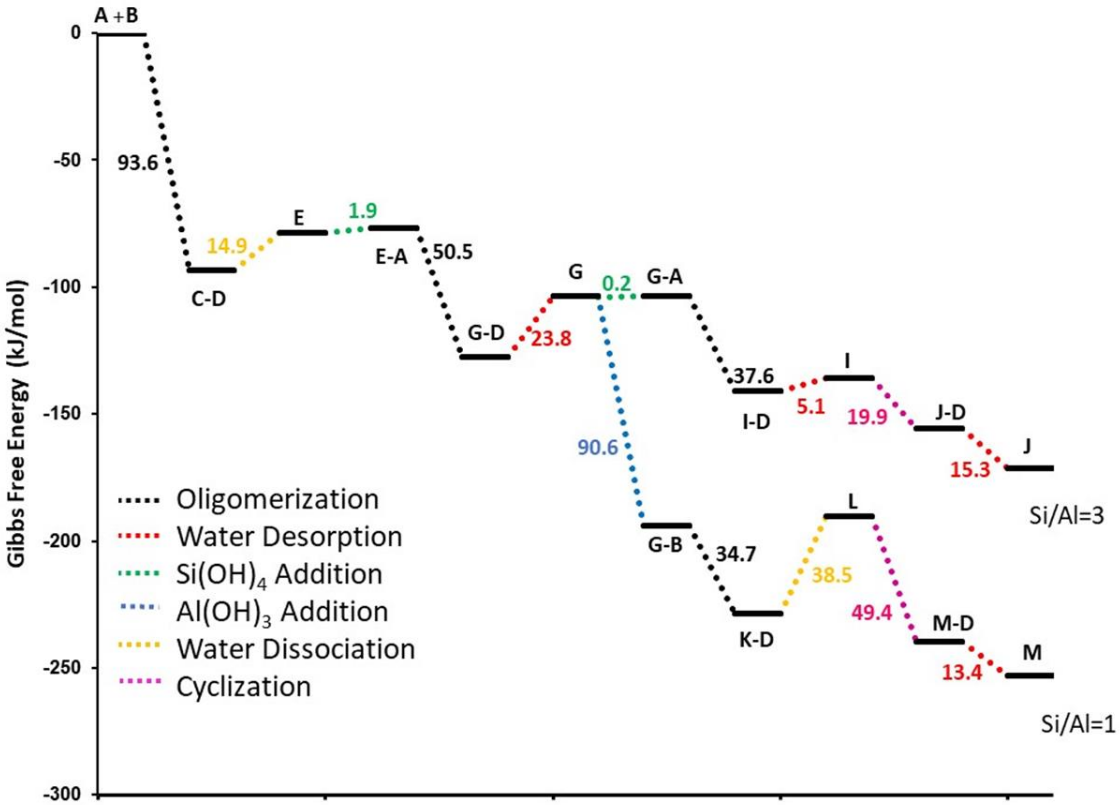


**Appendix Figure 19 Free energy reaction profile for oligomerization of aluminosilicate system. The alphabetically labeled states are used as a guide for the reaction extent data presented in Appendix Tables 7-10. The initial concentrations of Si and Al were 3 mols and 1 mol, and 2 mols and 2 mols, for the Si/Al=3 and Si/Al=1, respectively.**

**Appendix Table 7 Reaction extent data for each step in the oligomerization of the aluminosilicate system with Si/Al=3 up to formation of the cyclic trimer. Reaction species labeled A-J according to Appendix Figure 19.**

| Path to Tetramer | Reaction | Extent of Reaction (ξ) |
|---|---|---|
| 1 | A + B → C-D | 1.00 |
| 2 | C-D → E | 1.00 |
| 3 | E + A → E-A | 1.00 |
| 4 | E-A → G-D | 1.00 |
| 5 | G-D → G + D | 1.00 |
| 6 | G + A → G-A | 1.00 |
| 7 | G-A → I-D | 1.00 |
| 8 | I-D → I + D | 1.00 |
| 9 | I → J-D | 1.00 |
| 10 | J-D → J + D | 0.98 |

**Appendix Table 8 Number of final moles, molar Si and Al content, and total Si % and Al % of each species along the oligomerization pathway of the aluminosilicate system with Si/Al=3. Species designated A-J according to Appendix Figure 19.**

| | Species | $n_{final}$ | Si Content | Total Si % | Al Content | Total Al % |
|---|---|---|---|---|---|---|
| A | Si(OH)4 | 0.00 | 0.00 | 0.0 | 0.00 | 0.0 |
| B | Al(OH)3 | 0.00 | 0.00 | 0.0 | 0.00 | 0.0 |
| C-D | Si(OH)3-O-Al(OH)2--H2O | 0.00 | 0.00 | 0.0 | 0.00 | 0.0 |
| D | H2O | 2.98 | 0.00 | 0.0 | 0.00 | 0.0 |
| E | Si(OH)3-OH-Al(OH)3 | 0.00 | 0.00 | 0.0 | 0.00 | 0.0 |
| G | Si(OH)3-OH-Al(OH)2-O-Si(OH)3 | 0.00 | 0.00 | 0.0 | 0.00 | 0.0 |
| I | Si(OH)3-OH-Al(OH)2-O-Si(OH)2-O-Si(OH)4 | 0.00 | 0.00 | 0.0 | 0.00 | 0.0 |
| J | OSi(OH)2-OH-Al(OH)2-O-Si(OH)2-O-Si(OH)2 | 0.98 | 2.94 | 98.0 | 0.98 | 98.0 |
| E-A | Si(OH)3-OH-Al(OH)3--Si(OH)4 | 0.00 | 0.00 | 0.0 | 0.00 | 0.0 |
| G-A | Si(OH)3-OH-Al(OH)2-O-Si(OH)3--Si(OH)4 | 0.00 | 0.00 | 0.0 | 0.00 | 0.0 |
| G-D | Si(OH)3-OH-Al(OH)2-O-Si(OH)3--H2O | 0.00 | 0.00 | 0.0 | 0.00 | 0.0 |
| I-D | Si(OH)3-OH-Al(OH)2-O-Si(OH)2-O-Si(OH)3--H2O | 0.00 | 0.00 | 0.0 | 0.00 | 0.0 |
| J-D | OSi(OH)2-OH-Al(OH)2-O-Si(OH)2-O-Si(OH)2--H2O | 0.02 | 0.06 | 2.0 | 0.02 | 2.0 |

**Appendix Table 9 Reaction extent data for each step in the oligomerization of the aluminosilicate system with Si/Al=1 up to formation of the cyclic trimer. Reaction species labeled A-M according to Appendix Figure 19.**

| Path to Tetramer | Reaction | Extent of Reaction (ξ) |
|---|---|---|
| 1 | A + B → C-D | 1.00 |
| 2 | C-D → E | 1.00 |
| 3 | E + A → E-A | 1.00 |
| 4 | E-A → G-D | 1.00 |
| 5 | G-D → G + D | 1.00 |
| 6 | G + B → G-B | 1.00 |
| 7 | G-B → K-D | 1.00 |
| 8 | K-D → L | 0.43 |
| 9 | L → M-D | 0.42 |
| 10 | M-D → M + D | 0.42 |

**Appendix Table 10 Number of final moles, molar Si and Al content, and total Si % and Al % of each species along the oligomerization pathway of the aluminosilicate system with Si/Al=1. Species designated A-M according to Appendix Figure 19.**

| | Species | $n_{final}$ | Si Content | Total Si % | Al Content | Total Al % |
|---|---|---|---|---|---|---|
| A | Si(OH)4 | 0.00 | 0.00 | 0.0 | 0.00 | 0.0 |
| B | Al(OH)3 | 0.00 | 0.00 | 0.0 | 0.00 | 0.0 |
| C-D | Si(OH)3-O-Al(OH)2--H2O | 0.00 | 0.00 | 0.0 | 0.00 | 0.0 |
| D | H2O | 1.42 | 0.00 | 0.0 | 0.00 | 0.0 |
| E | Si(OH)3-OH-Al(OH)3 | 0.00 | 0.00 | 0.0 | 0.00 | 0.0 |
| G | Si(OH)3-OH-Al(OH)2-O-Si(OH)3 | 0.00 | 0.00 | 0.0 | 0.00 | 0.0 |
| L | Si(OH)3-OH-Al(OH)2-O-Si(OH)2-OH-Al(OH)3 | 0.01 | 0.00 | 0.0 | 0.00 | 0.0 |
| M | OSi(OH)2-OH-Al(OH)2-O-Si(OH)2-OH-Al(OH)2 | 0.42 | 0.84 | 42.0 | 0.84 | 42.0 |
| E-A | Si(OH)3-OH-Al(OH)3--Si(OH)4 | 0.00 | 0.00 | 0.0 | 0.00 | 0.0 |
| G-D | Si(OH)3-OH-Al(OH)2-O-Si(OH)3--H2O | 0.00 | 0.00 | 0.0 | 0.00 | 0.0 |
| G-B | Si(OH)3-OH-Al(OH)2-O-Si(OH)3--Al(OH)3 | 0.00 | 0.00 | 0.0 | 0.00 | 0.0 |
| K-D | Si(OH)3-OH-Al(OH)2-O-Si(OH)2-O-Al(OH)2--H2O | 0.57 | 1.14 | 57.0 | 1.14 | 57.0 |
| M-D | OSi(OH)2-OH-Al(OH)2-O-Si(OH)2-OH-Al(OH)2--H2O | 0.01 | 0.02 | 1.0 | 0.02 | 1.0 |

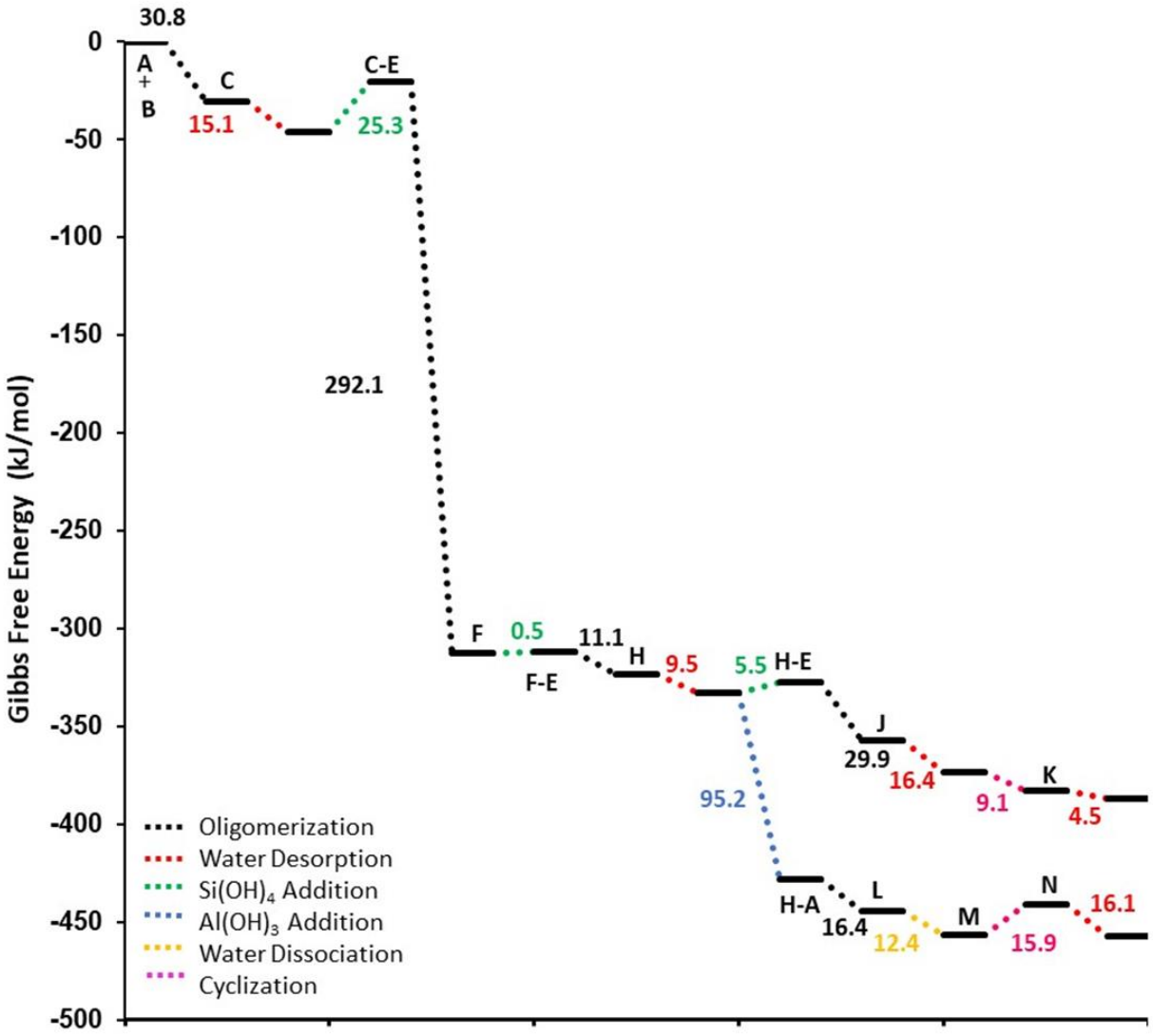


**Appendix Figure 20 Free energy reaction profile for oligomerization of aluminosilicate system in the presence of NaOH. The alphabetically labeled states are used as a guide for the reaction extent data presented in Appendix Tables 11-14. Initial concentrations of Si, Al and Na were 3 mols Si, 1 mol Al, and 1 mol Na for the Si/Al=3 path, and 2 mols Si, 2 mols Al, and 1 mol Na for the Si/Al=1 pathway.**

**Appendix Table 11 Reaction extent data for each step in the oligomerization of the aluminosilicate system in the presence of NaOH with Si/Al=3 up to formation of the cyclic trimer. Reaction species labeled A-K according to Appendix Figure 20.**

| Path to Tetramer | Reaction | Extent of Reaction (ξ) |
|---|---|---|
| 1 | A+ B → C-D | 0.99 |
| 2 | C-D → C + D | 0.98 |
| 3 | C + E → C-E | 0.98 |
| 4 | C-E → F | 0.98 |
| 5 | F + E → F-E | 0.98 |
| 6 | F-E → H-D | 0.98 |
| 7 | H-D → H + D | 0.98 |
| 8 | H + E → H-E | 0.98 |
| 9 | H-E → J-D | 0.98 |
| 10 | J-D → J + D | 0.98 |
| 11 | J → K-D | 0.98 |
| 12 | K-D → K + D | 0.98 |

**Appendix Table 12 Number of final moles, molar Si, Al, and Na content, and total Si %, Al %, and Na % of each species along the oligomerization pathway of the aluminosilicate system with Si/Al=3. Species designated A-K according to Appendix Figure 20.**

| | Species | $n_{final}$ | Si Content | Total Si % | Al Content | Total Al % | Na Content | Total Na % |
|---|---|---|---|---|---|---|---|---|
| A | Al(OH)3 | 0.01 | 0.00 | 0.0 | 0.01 | 1.0 | 0.00 | 0.0 |
| B | NaOH | 0.01 | 0.00 | 0.0 | 0.00 | 0.0 | 0.01 | 1.0 |
| C | Al(OH)2ONa | 0.00 | 0.00 | 0.0 | 0.00 | 0.0 | 0.00 | 0.0 |
| D | H2O | 3.92 | 0.00 | 0.0 | 0.00 | 0.0 | 0.00 | 0.0 |
| E | Si(OH)4 | 0.06 | 0.06 | 2.0 | 0.00 | 0.0 | 0.00 | 0.0 |
| F | Si(OH)3-ONa-Al(OH)3 | 0.00 | 0.00 | 0.0 | 0.00 | 0.0 | 0.00 | 0.0 |
| H | Si(OH)3-ONa-Al(OH)2-O-Si(OH)3 | 0.00 | 0.00 | 0.0 | 0.00 | 0.0 | 0.00 | 0.0 |
| J | Si(OH)3-ONa-Al(OH)2-O-Si(OH)2-O-Si(OH)3 | 0.00 | 0.00 | 0.0 | 0.00 | 0.0 | 0.00 | 0.0 |
| K | OSi(OH)2-ONa-Al(OH)2-O-Si(OH)2-O-Si(OH)2 | 0.98 | 2.94 | 98.0 | 0.98 | 98.0 | 0.98 | 98.0 |
| C-D | Al(OH)2ONa--H2O | 0.01 | 0.00 | 0.0 | 0.01 | 1.0 | 0.01 | 1.0 |
| C-E | Al(OH)2ONa--Si(OH)4 | 0.00 | 0.00 | 0.0 | 0.00 | 0.0 | 0.00 | 0.0 |
| F-E | Si(OH)3-ONa-Al(OH)3--Si(OH)4 | 0.00 | 0.00 | 0.0 | 0.00 | 0.0 | 0.00 | 0.0 |
| H-D | Si(OH)3-ONa-Al(OH)2-O-Si(OH)3--H2O | 0.00 | 0.00 | 0.0 | 0.00 | 0.0 | 0.00 | 0.0 |
| H-E | Si(OH)3-ONa-Al(OH)2-O-Si(OH)3--Si(OH)4 | 0.00 | 0.00 | 0.0 | 0.00 | 0.0 | 0.00 | 0.0 |
| J-D | Si(OH)3-ONa-Al(OH)2-O-Si(OH)2-O-Si(OH)3--H2O | 0.00 | 0.00 | 0.0 | 0.00 | 0.0 | 0.00 | 0.0 |
| K-D | OSi(OH)2-ONa-Al(OH)2-O-Si(OH)2-O-Si(OH)2--H2O | 0.00 | 0.00 | 0.0 | 0.00 | 0.0 | 0.00 | 0.0 |

**Appendix Table 13 Reaction extent data for each step in the oligomerization of the aluminosilicate system in the presence of NaOH with Si/Al=1 up to formation of the cyclic trimer. Reaction species labeled A-N according to Appendix Figure 20.**

| Path to Tetramer | Reaction | Extent of Reaction (ξ) |
|---|---|---|
| 1 | A+ B → C-D | 1.00 |
| 2 | C-D → C + D | 1.00 |
| 3 | C + E → C-E | 1.00 |
| 4 | C-E → F | 1.00 |
| 5 | F + E → F-E | 1.00 |
| 6 | F-E → H-D | 1.00 |
| 7 | H-D → H + D | 1.00 |
| 8 | H + A → H-A | 1.00 |
| 9 | H-A → L-D | 1.00 |
| 10 | L-D →M | 0.99 |
| 11 | M →N-D | 0.51 |
| 12 | N-D →N + D | 0.50 |

**Appendix Table 14 Tabulation of final moles, molar Si, Al, and Na content, and total Si %, Al %, and Na % of each species along the oligomerization pathway of the aluminosilicate system with Si/Al=1. Species designated A-N according to Appendix Figure 20.**

| | Species | $n_{final}$ | Si Content | Total Si % | Al Content | Total Al % | Na Content | Total Na % |
|---|---|---|---|---|---|---|---|---|
| A | Al(OH)3 | 0.00 | 0.00 | 0.0 | 0.00 | 0.0 | 0.00 | 0.0 |
| B | NaOH | 0.00 | 0.00 | 0.0 | 0.00 | 0.0 | 0.00 | 0.0 |
| C | Al(OH)2ONa | 0.00 | 0.00 | 0.0 | 0.00 | 0.0 | 0.00 | 0.0 |
| D | H2O | 2.50 | 0.00 | 0.0 | 0.00 | 0.0 | 0.00 | 0.0 |
| E | Si(OH)4 | 0.00 | 0.00 | 0.0 | 0.00 | 0.0 | 0.00 | 0.0 |
| F | Si(OH)3-ONa-Al(OH)3 | 0.00 | 0.00 | 0.0 | 0.00 | 0.0 | 0.00 | 0.0 |
| H | Si(OH)3-ONa-Al(OH)2-O-Si(OH)3 | 0.00 | 0.00 | 0.0 | 0.00 | 0.0 | 0.00 | 0.0 |
| M | Si(OH)3-ONa-Al(OH)2-O-Si(OH)2-OH-Al(OH)3 | 0.49 | 0.98 | 49.0 | 0.98 | 49.0 | 0.49 | 49.0 |
| N | OSi(OH)2-ONa-Al(OH)2-O-Si(OH)2-OH-Al(OH)2 | 0.50 | 1.00 | 50.0 | 1.00 | 50.0 | 0.50 | 50.0 |
| C-D | Al(OH)2ONa--H2O | 0.00 | 0.00 | 0.0 | 0.00 | 0.0 | 0.00 | 0.0 |
| C-E | Al(OH)2ONa--Si(OH)4 | 0.00 | 0.00 | 0.0 | 0.00 | 0.0 | 0.00 | 0.0 |
| F-E | Si(OH)3-ONa-Al(OH)3--Si(OH)4 | 0.00 | 0.00 | 0.0 | 0.00 | 0.0 | 0.00 | 0.0 |
| H-D | Si(OH)3-ONa-Al(OH)2-O-Si(OH)3--H2O | 0.00 | 0.00 | 0.0 | 0.00 | 0.0 | 0.00 | 0.0 |
| H-A | Si(OH)3-ONa-Al(OH)2-O-Si(OH)3--Al(OH)3 | 0.00 | 0.00 | 0.0 | 0.00 | 0.0 | 0.00 | 0.0 |
| L-D | Si(OH)3-ONa-Al(OH)2-O-Si(OH)2-O-Al(OH)2--H2O | 0.01 | 0.02 | 1.0 | 0.02 | 1.0 | 0.01 | 1.0 |
| N-D | OSi(OH)2-ONa-Al(OH)2-O-Si(OH)2-OH-Al(OH)2--H2O | 0.00 | 0.00 | 0.0 | 0.00 | 0.0 | 0.00 | 0.0 |

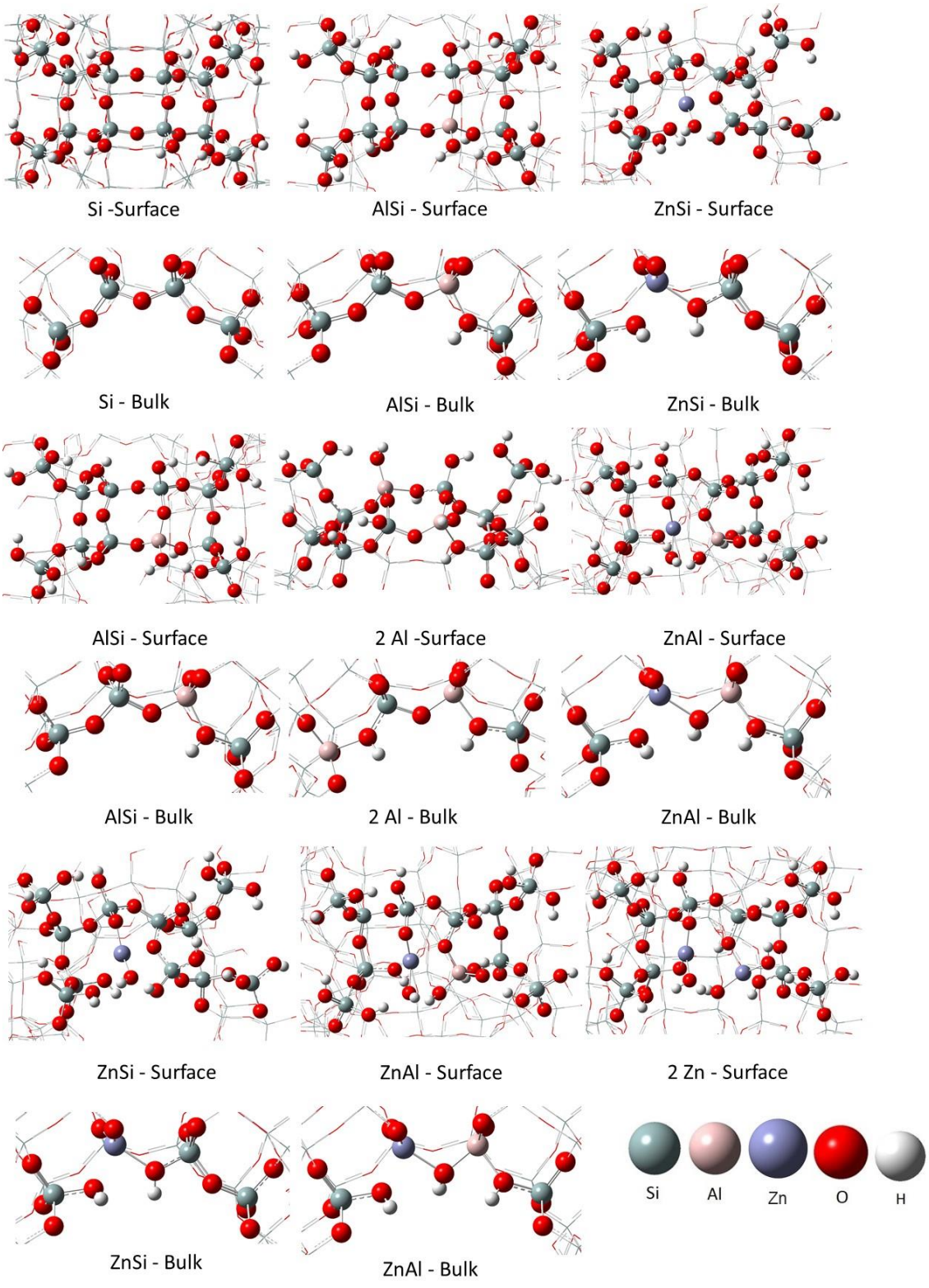


**Appendix Figure 21 Structures for each initial and substituted state included in Table 1. States are arranged in the same order and correspond to each Gibbs free energy given in Table 1.**

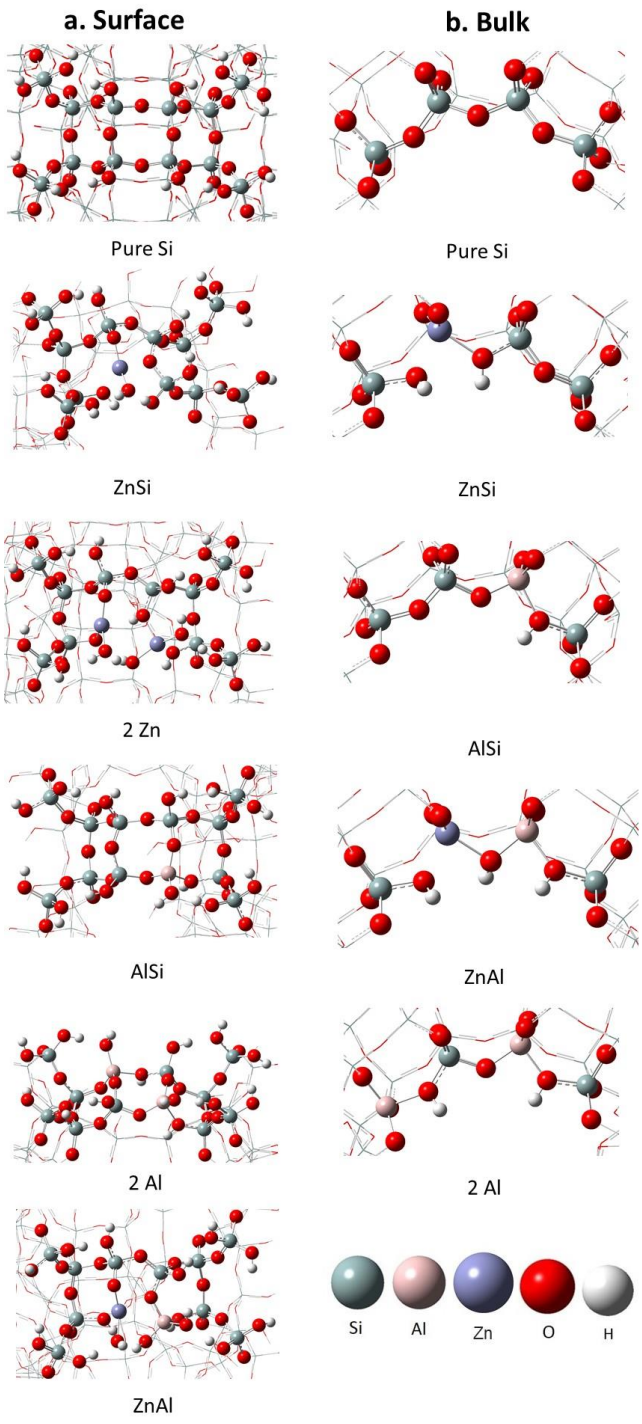


**Appendix Figure 22 Structures for each state given on the reaction profiles of a) surface and b) bulk systems included in Figure 7. Structures are labeled to correspond to labels of states in Figure 7.**

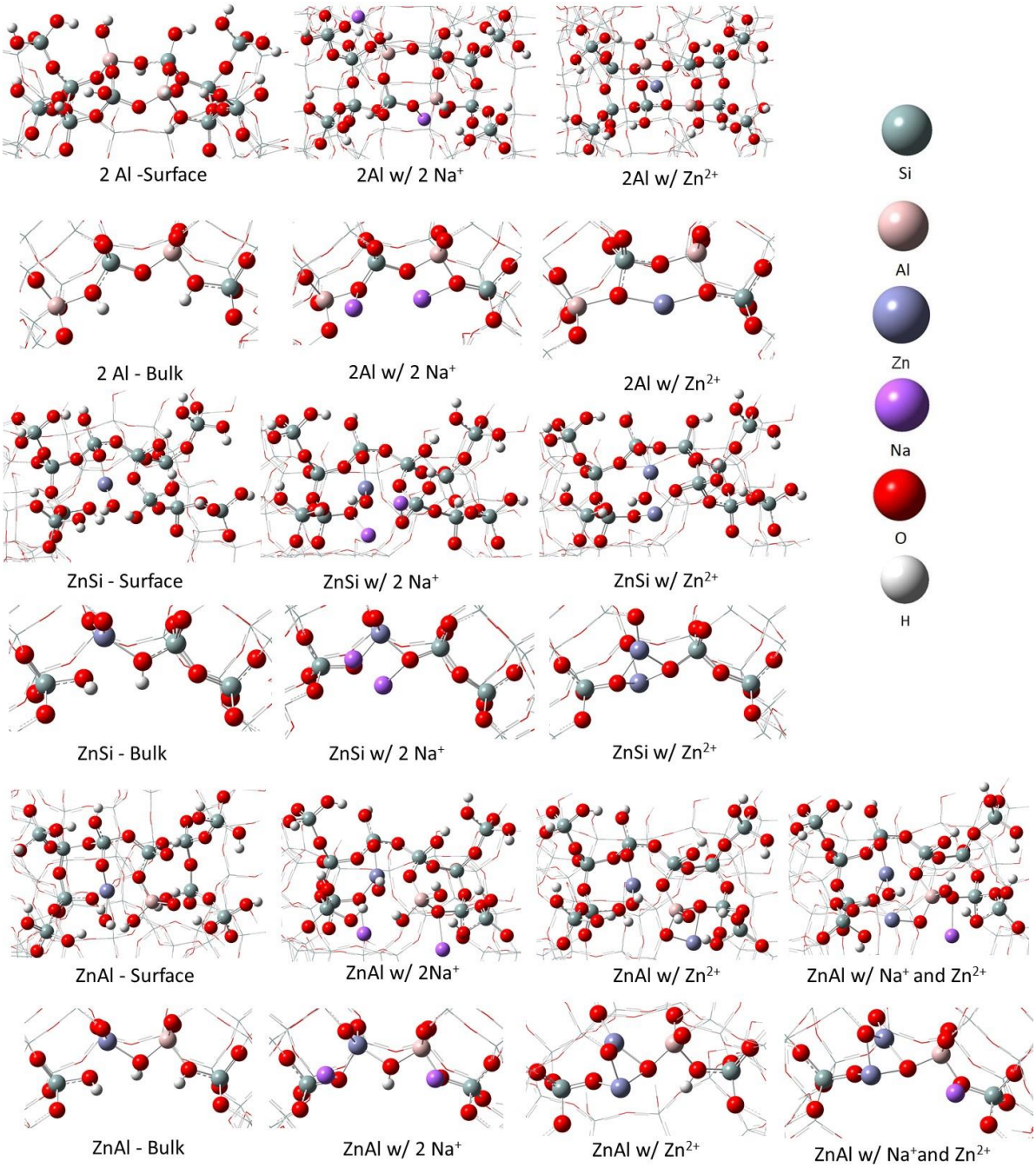


**Appendix Figure 23 Structures for each initial and substituted state included in Table 2. States are arranged in the same order and correspond to each Gibbs free energy given in Table 2.**

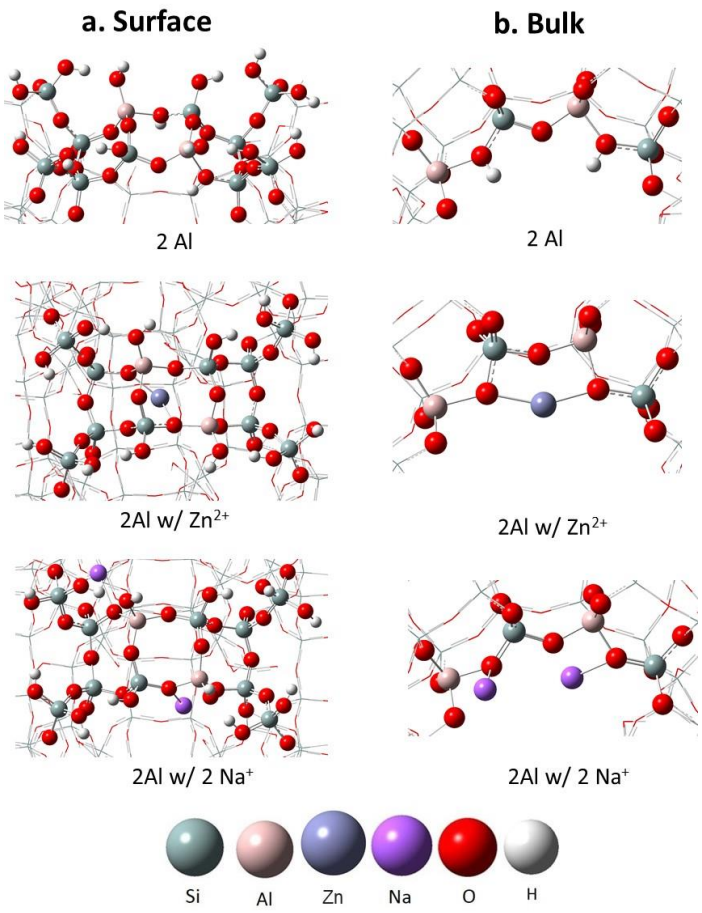


**Appendix Figure 24 Structures for each state given on the reaction profiles of a) surface and b) bulk systems included in Figure 8. Structures are labeled to correspond to labels of states in Figure 8.**

## Bibliography


**1.** Ates A, Akgul G. Modification of natural zeolite with NaOH for removal of manganese in drinking water. *Powder Technology.* Jan 2016;287:285-291.

**2.** Liu Y, Yan CJ, Zhao JJ, et al. Synthesis of zeolite P1 from fly ash under solvent-free conditions for ammonium removal from water. *Journal of Cleaner Production.* Nov 2018;202:11-22.

**3.** Zaker A, Guerra P, Wang YP, et al. Evidence of heterogeneous catalytic activity of ZSM-5 in supercritical water for dodecane cracking. *Catalysis Today.* Nov 2018;317:2-11.

**4.** Rahimi N, Karimzadeh R. Catalytic cracking of hydrocarbons over modified ZSM-5 zeolites to produce light olefins: A review. *Applied Catalysis a-General.* May 2011;398(1-2):1-17.

**5.** Baron J, Herzog S. Public opinion on nuclear energy and nuclear weapons: The attitudinal nexus in the United States. *Energy Research & Social Science.* 2020/10/01/ 2020;68:101567.

**6.** Strachan DM, Neeway JJ. Effects of alteration product precipitation on glass dissolution. *Applied Geochemistry.* 2014/06/01/ 2014;45:144-157.

**7.** Parruzot B, Ryan JV, George JL, et al. Multi-glass investigation of Stage III glass dissolution behavior from 22 to 90 °C triggered by the addition of zeolite phases. *Journal of Nuclear Materials.* 2019/09/01/ 2019;523:490-501.

**8.** Neeway JJ, Parruzot BP, Bonnett JF, et al. Acceleration of glass alteration rates induced by zeolite seeds at controlled pH. *Applied Geochemistry.* 2020/02/01/ 2020;113:104515.

**9.** Fournier M, Gin S, Frugier P, Mercado-Depierre S. Contribution of zeolite-seeded experiments to the understanding of resumption of glass alteration. *npj Materials Degradation.* 2017/11/13 2017;1(1):17.

**10.** Fournier M, Gin S, Frugier P. Resumption of nuclear glass alteration: State of the art. *Journal of Nuclear Materials.* May 2014;448(1-3):348-363.

**11.** Gin S, Mestre JP. SON 68 Nuclear Glass Alteration Kinetics between pH 7 and pH 11.5. *Journal of Nuclear Materials.* 05/01 2001;295:83–96.

**12.** Majérus O, Lehuédé P, Biron I, Alloteau F, Narayanasamy S, Caurant D. Glass alteration in atmospheric conditions: crossing perspectives from cultural heritage, glass industry, and nuclear waste management. *npj Materials Degradation.* 2020/08/27 2020;4(1):27.

**13.** Mallants D, Chapman N. How much does corrosion of nuclear waste matrices matter. *Nature Materials.* 2020/09/01 2020;19(9):959-961.

**14.** de Moor P, Beelen TPM, van Santen RA, Beck LW, Davis ME. Si-MFI crystallization using a "dimer" and "trimer" of TPA studied with small-angle X-ray scattering. *Journal of Physical Chemistry B.* Aug 2000;104(32):7600-7611.

**15.** Freeman EE, Neeway JJ, Motkuri RK, Rimer JD, Mpourmpakis G. Understanding initial zeolite oligomerization steps with first principles calculations. *Aiche Journal.* Dec 2020;66(12).

**16.** Knight CTG, Balec RJ, Kinrade SD. The structure of silicate anions in aqueous alkaline solutions. *Angewandte Chemie-International Edition.* 2007;46(43):8148-8152.

**17.** Mora-Fonz MJ, Catlow CRA, Lewis DW. Oligomerization and cyclization processes in the nucleation of microporous silicas. *Angewandte Chemie-International Edition.* 2005;44(20):3082-3086.
**18.** Mora-Fonz MJ, Hamad S, Catlow CRA. Modelling nucleation and nano-particle structures. *Molecular Physics.* Jan-Feb 2007;105(2-3):177-187.
**19.** Pereira JCG, Catlow CRA, Price GD. Ab initio studies of silica-based clusters. Part I. Energies and conformations of simple clusters. *Journal of Physical Chemistry A.* Apr 1999;103(17):3252-3267.
**20.** Gomes JRB, Cordeiro M, Jorge M. Gas-phase molecular structure and energetics of anionic silicates. *Geochimica Et Cosmochimica Acta.* Sep 2008;72(17):4421-4439.
**21.** Zhang XQ, Trinh TT, van Santen RA, Jansen APJ. Mechanism of the Initial Stage of Silicate Oligomerization. *Journal of the American Chemical Society.* May 2011;133(17):6613-6625.
**22.** Liu X, Liu C, Meng CG. Oligomerization of Silicic Acids in Neutral Aqueous Solution: A First-Principles Investigation. *International Journal of Molecular Sciences.* Jun 2019;20(12).
**23.** Moqadam M, Riccardi E, Trinh TT, Lervik A, van Erp TS. Rare event simulations reveal subtle key steps in aqueous silicate condensation. *Physical Chemistry Chemical Physics.* May 2017;19(20):13361-13371.
**24.** Zhang XQ, van Santen RA, Jansen APJ. Kinetic Monte Carlo modeling of silicate oligomerization and early gelation. *Physical Chemistry Chemical Physics.* 2012;14(34):11969-11973.
**25.** Grand J, Awala H, Mintova S. Mechanism of zeolites crystal growth: new findings and open questions. *Crystengcomm.* 2016;18(5):650-664.
**26.** Mpourmpakis G, Vlachos DG. Insights into the early stages of metal nanoparticle formation via first-principle calculations: the roles of citrate and water. *Langmuir.* Jul 2008;24(14):7465-7473.
**27.** White CE, Provis JL, Kearley GJ, Riley DP, van Deventer JSJ. Density functional modelling of silicate and aluminosilicate dimerisation solution chemistry. *Dalton Transactions.* 2011;40(6):1348-1355.
**28.** Van Speybroeck V, Hemelsoet K, Joos L, Waroquier M, Bell RG, Catlow CRA. Advances in theory and their application within the field of zeolite chemistry. *Chemical Society Reviews.* 2015;44(20):7044-7111.
**29.** Catlow CRA, Bromley ST, Hamad S, Mora-Fonz M, Sokol AA, Woodley SM. Modelling nano-clusters and nucleation. *Physical Chemistry Chemical Physics.* 2010;12(4):786-811.
**30.** Zhang XQ, Trinh TT, van Santen RA, Jansen APJ. Structure-Directing Role of Counterions in the Initial Stage of Zeolite Synthesis. *Journal of Physical Chemistry C.* May 2011;115(19):9561-9567.
**31.** Bosnar S, Antonic T, Bronic J, Subotic B. Mechanism and kinetics of the growth of zeolite microcrystals. Part 2: Influence of sodium ions concentration in the liquid phase on the growth kinetics of zeolite A microcrystals. *Microporous and Mesoporous Materials.* Dec 2004;76(1-3):157-165.
**32.** Anseau MR, Leung JP, Sahal N, Swaddle TW. Interactions of silicate ions with zinc(II) and aluminum(III) in alkaline aqueous solution. *Inorganic Chemistry.* Oct 2005;44(22):8023-8032.

**33.** Hikichi N, Iyoki K, Naraki Y, et al. Role of sodium cation during aging process in the synthesis of LEV-type zeolite. *Microporous and Mesoporous Materials.* Aug 2019;284:82-89.
**34.** Muraoka K, Sada Y, Miyazaki D, Chaikittisilp W, Okubo T. Linking synthesis and structure descriptors from a large collection of synthetic records of zeolite materials. *Nature communications.* 2019;10(1):1-11.
**35.** Osuga R, Bayarsaikhan S, Yasuda S, et al. Metal cation-exchanged zeolites with the location, state, and size of metal species controlled. *Chemical Communications.* 2020;56(44):5913-5916.
**36.** Petitjean H, Lepetit C, Nour Z, Poteau R, del Rosal I, Berthomieu De. How CuI and NaI Interact with Faujasite Zeolite? A Theoretical Investigation. *The Journal of Physical Chemistry C.* 2020.
**37.** Heard CJ, Grajciar L, Uhlík F, et al. Zeolite (In) Stability under Aqueous or Steaming Conditions. *Advanced Materials.* 2020;32(44):2003264.
**38.** Zheng H, Narkhede N, Zhang G, Li Z. Role of metal co-cations in improving CuY zeolite performance for DMC synthesis: A theoretical study. *Applied Organometallic Chemistry.* 2020;34(10):e5832.
**39.** Schwalbe-Koda D, Jensen Z, Olivetti E, Gómez-Bombarelli R. Graph similarity drives zeolite diffusionless transformations and intergrowth. *Nature materials.* 2019;18(11):1177-1181.
**40.** Suhendar D, Mukti R. Simple approach in understanding interzeolite transformations using ring building units. Paper presented at: IOP Conference Series: Materials Science and Engineering2018.
**41.** *Gaussian 09, Revision D.01* [computer program]. Wallingford CT: Gaussian, Inc.; 2013.
**42.** Zhao Y, Truhlar DG. The M06 suite of density functionals for main group thermochemistry, thermochemical kinetics, noncovalent interactions, excited states, and transition elements: two new functionals and systematic testing of four M06-class functionals and 12 other functionals. *Theoretical Chemistry Accounts.* May 2008;120(1-3):215-241.
**43.** Zhao Y, Truhlar DG. Density functionals with broad applicability in chemistry. *Accounts of Chemical Research.* Feb 2008;41(2):157-167.
**44.** Takano Y, Houk KN. Benchmarking the conductor-like polarizable continuum model (CPCM) for aqueous solvation free energies of neutral and ionic organic molecules. *Journal of Chemical Theory and Computation.* Jan-Feb 2005;1(1):70-77.
**45.** Besora M, Vidossich P, Lledos A, Ujaque G, Maseras F. Calculation of Reaction Free Energies in Solution: A Comparison of Current Approaches. *Journal of Physical Chemistry A.* Feb 2018;122(5):1392-1399.
**46.** Feng S, Bagia C, Mpourmpakis G. Determination of Proton Affinities and Acidity Constants of Sugars. *The Journal of Physical Chemistry A.* 2013/06/20 2013;117(24):5211-5219.
**47.** Stewart JJ. Application of the PM6 method to modeling the solid state. *Journal of molecular modeling.* 2008;14(6):499-535.
**48.** Oleksiak MD, Ghorbanpour A, Conato MT, et al. Synthesis Strategies for Ultrastable Zeolite GIS Polymorphs as Sorbents for Selective Separations. *Chemistry-a European Journal.* Nov 2016;22(45):16078-16088.

**49.** Loewenstein W. The distribution of aluminum in the tetrahedra of silicates and aluminates. *American Mineralogist.* 1954;39(1-2):92-96.
**50.** Trinh TT, Jansen APJ, van Santen RA. Mechanism of oligomerization reactions of silica. *Journal of Physical Chemistry B.* Nov 2006;110(46):23099-23106.
**51.** Shirazi L, Jamshidi E, Ghasemi MR. The effect of Si/Al ratio of ZSM-5 zeolite on its morphology, acidity and crystal size. *Crystal Research and Technology.* Dec 2008;43(12):1300-1306.
**52.** Qi CC, Liu L, He JY, Chen QS, Yu LJ, Liu PF. Understanding Cement Hydration of Cemented Paste Backfill: DFT Study of Water Adsorption on Tricalcium Silicate (111) Surface. *Minerals.* Apr 2019;9(4):17.
**53.** Wang Q, Manzano H, Guo Y, Lopez-Arbeloa I, Shen X. Hydration Mechanism of Reactive and Passive Dicalcium Silicate Polymorphs from Molecular Simulations. *The Journal of Physical Chemistry C.* 2015/08/27 2015;119(34):19869-19875.
**54.** Guo P, Wang B, Bauchy M, Sant G. Misfit Stresses Caused by Atomic Size Mismatch: The Origin of Doping-Induced Destabilization of Dicalcium Silicate. *Crystal Growth & Design.* 2016/06/01 2016;16(6):3124-3132.
**55.** Claverie J, Bernard F, Cordeiro JMM, Kamali-Bernard S. Water's behaviour on Ca-rich tricalcium silicate surfaces for various degrees of hydration: A molecular dynamics investigation. *J. Phys. Chem. Solids.* Sep 2019;132:48-55.
**56.** Harris R, Knight C, Hull W. Nature of species present in an aqueous solution of potassium silicate. *Journal of the American Chemical Society.* 1981;103(6):1577-1578.
**57.** Kirschhock CEA, Ravishankar R, Verspeurt F, Grobet PJ, Jacobs PA, Martens JA. Identification of Precursor Species in the Formation of MFI Zeolite in the TPAOH−TEOS−H2O System. *The Journal of Physical Chemistry B.* 1999/06/01 1999;103(24):4965-4971.
**58.** Ciantar M, Mellot-Draznieks C, Nieto-Draghi C. A kinetic monte carlo simulation study of synthesis variables and diffusion coefficients in early stages of silicate oligomerization. *The Journal of Physical Chemistry C.* 2015;119(52):28871-28884.
**59.** Lim IH, Schrader W, Schüth F. The formation of zeolites from solution – Analysis by mass spectrometry. *Microporous and Mesoporous Materials.* 2013/01/15/ 2013;166:20-36.
**60.** Pelster SA, Kalamajka R, Schrader W, Schüth F. Monitoring the Nucleation of Zeolites by Mass Spectrometry. *Angewandte Chemie International Edition.* 2007/03/19 2007;46(13):2299-2302.
**61.** McCusker CBaLB. Database of Zeolite Structures:
.
**62.** Baur WH. On the cation and water positions in faujasite. *American Mineralogist: Journal of Earth and Planetary Materials.* 1964;49(5-6):697-704.